Modelling of surface stresses and fracturing during dyke emplacement: Application to the 2009 episode at Harrat Lunayyir, Saudi Arabia

Azizah Al Shehri and Agust Gudmundsson

Department of Earth Sciences, Royal Holloway University of London, Egham, UK

Abstract

Correct interpretation of surface stresses and deformation or displacement during volcanotectonic episodes is of fundamental importance for hazard assessment and dyke-path forecasting. Here we present new general numerical models on the local stresses induced by arrested dykes. In the models, the crustal segments hosting the dyke vary greatly in mechanical properties, from uniform or non-layered (elastic half-spaces) to highly anisotropic (layers with strong contrast in Young's modulus). The shallow parts of active volcanoes and volcanic zones are normally highly anisotropic and some with open contacts. The numerical results show that, for a given surface deformation, non-layered (half-space) models underestimate the dyke overpressure/thickness needed and overestimate the likely depth to the tip of the dyke. Also, as the mechanical contrast between the layers increases, so does the stress dissipation and associated reduction in surface stresses (and associated fracturing). In the absence of open contacts, the distance between the two dyke-induced tensile and shear stress peaks (and fractures, if any) at the surface is roughly twice the depth to the tip of the dyke. The width of a graben, if it forms, should therefore be roughly twice the depth to the tip of the associated arrested dyke. When applied to the 2009 episode at Harrat Lunayyir, the main results are as follows. The entire 3-7 km wide fracture zone/graben formed during the episode is far too wide to have been generated by induced stresses of a single, arrested dyke. The eastern part of the zone/graben may have been generated by the inferred, arrested dyke, but the western zone primarily by regional extensional loading. The dyke tip was arrested at only a few hundred metres below the surface, the estimated thickness of the uppermost part of the dyke being between about 6 and 12 m. For the inferred dyke length (strike dimension) of about 14 km, this yields a dyke length/thickness ratio between 2400 and 1200, similar to commonly measured ratios of regional dykes in the field.

Keywords: Dyke propagation, dyke arrest, surface deformation, grabens, crustal stresses, numerical models

1. Introduction

Most volcanic eruptions occur when a magma-filled fracture is able to propagate from its source to the surface. In many central volcanoes (composite volcanoes/stratovolcanoes and collapse calderas) the source is a shallow magma chamber, in which case the local stress field may favour inclined (cone) sheets rather than vertical dykes. In areas of rifting outside central volcanoes, however, the regional stress field controls the magma propagation path. In rift

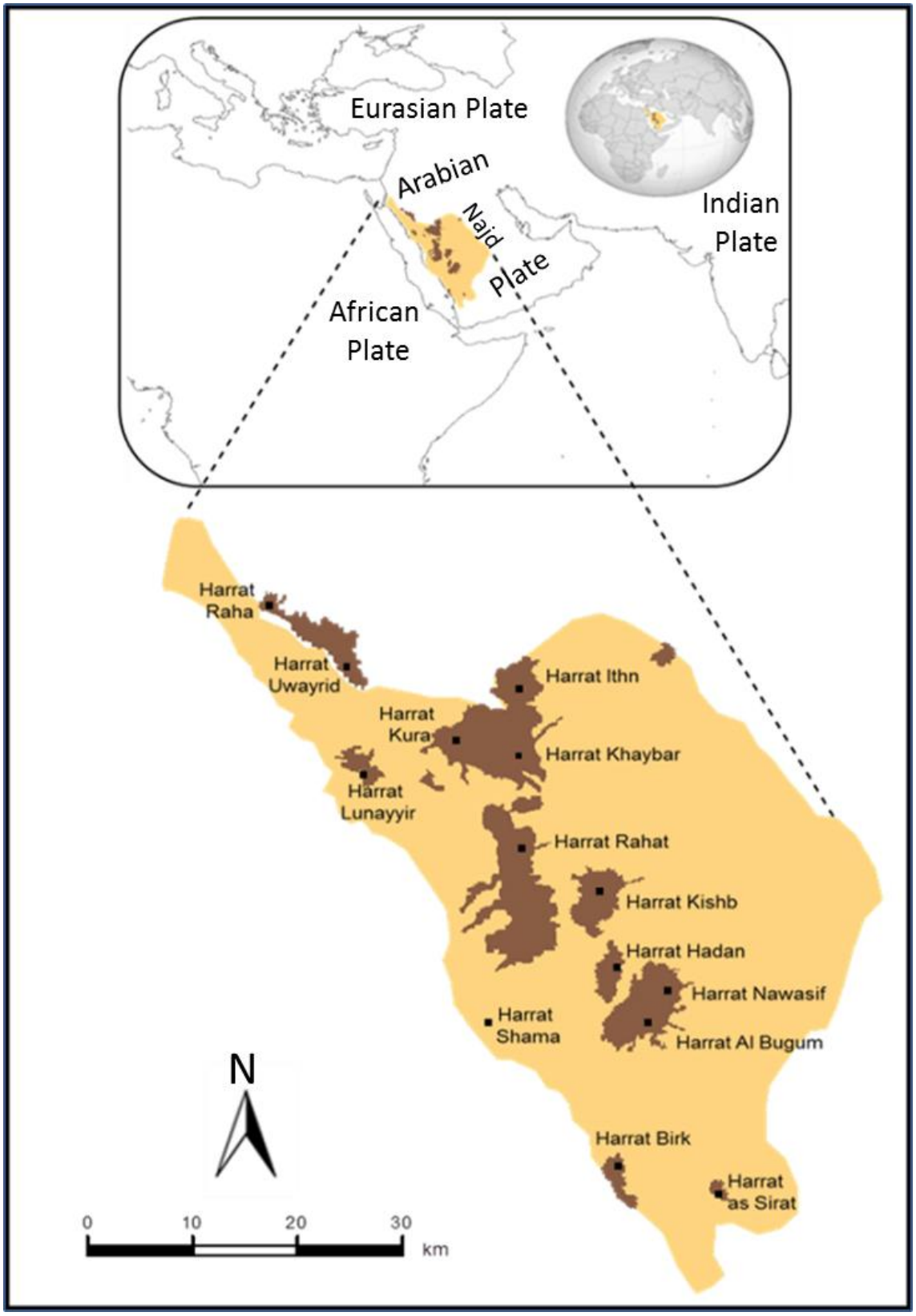

Fig. 1. *Main Cenozoic lava files (referred to as harrats) in western Saudi Arabia (their location in a wider geographic context is on the inset). Modified from a map of the SGS (https://www.sgs.org.sa, 2011).*

zones the minimum principal compressive stress σ_3 is normally horizontal and parallel with the spreading or rifting vector. Since all magma-filled fractures generally form perpendicular to the σ_3 it follows that the greater parts of magma paths tend to be vertical dykes.

Most dykes (and inclined sheets) do not reach the surface to erupt but rather become arrested (stop their propagation path, stall) at various depths in the crust (Gudmundsson, 2002, 2003; Moran et al., 2011; Rivalta et al., 2015; Townsend et al., 2017). The conditions for dyke arrest have been studied in the field (Gudmundsson, 2002, 2003; Gudmundsson and Philipp, 2006; Tibaldi, 2015) and through analogue models (Kvanagh et al., 2006), numerical models (Gudmundsson and Philipp, 2006; Barnett and Gudmundsson, 2014; Rivalta et al., 2015; Townsend et al., 2017), and analytical models (Gudmundsson, 2011a,b). Understanding these conditions is of fundamental importance in theoretical and applied volcanology. Despite all the available instrumentation for volcano monitoring, we still cannot forecast dyke-propagation paths once a dyke has been initiated during magma-chamber/reservoir rupture. It follows that we cannot make reliable forecasts as to (i) what the likely path of the dyke is going to be and, in particular, (ii) whether or not the dyke is going to reach the surface and erupt or, alternatively, (iii) become arrested at some depth in the volcano. Direct field studies of arrested solidified or 'frozen' dykes, as well as geodetic and seismic studies of dyke arrest during unrest periods, are of great importance for improving our understanding of dyke propagation and dyke-fed eruptions.

There have been many reported dyke arrests in recent decades. In some unrest periods many dykes have become arrested while at the end of the unrest period one or more dykes have reached the surface to erupt. A well-documented case of this type is the unrest in the volcano Eyjafjallajökull in South Iceland for nearly two decades before its 2010 eruption. During the period 1993 until 2010 there were 4-5 dyke injections that became arrested, some of the dykes changing into sills, until in March 2010 a new dyke injection reached the surface and erupted (Sigmundsson et al., 2010). Many dykes and sills are exposed in the volcano, suggesting that episodes of this kind are common (Gudmundsson, 2017). Many unrest periods with dyke injections, however, have not resulted in eruptions. One happened in Tenerife, Canary Islands, in 2004 (Garcia et al., 2006; Gottsmann et al., 2006), and another one in Harrat Lunayyir in western Saudi Arabia in 2009 (Baer and Hamiel, 2010; Pallister et al., 2010; Xu et al., 2016). This latter one is the main topic of the present paper.

This paper has two aims. The first is to present new and general results on dyke-induced stresses in crustal segments with contrasting mechanical properties. Here the focus is on new numerical models on dykes arrested with their tips at various crustal depths and hosted by rocks with mechanical properties that range from elastic half spaces (uniform properties) to those with alternating stiff (high Young's modulus) and soft (compliant, low Young's modulus) layers. The results are completely general, but are here applied to the 2009 volcanotectonic unrest period in Harrat Lunayyir in Saudi Arabia (Figs. 1 and 2). The second, and main, aim is thus to use the numerical results, as well as some analytical models together with field observations of the associated surface deformation, to make new estimates of the dimensions, the depth to the tip at arrest, and contribution to surface deformation of the dyke inferred to have been emplaced during the 2009 episode. We also put the dyke propagation and arrest in Harrat Lunayyir into general context of arrested dykes, their dimensions, and aspect (length/thickness) ratios, as obtained in direct field studies. Furthermore, we explain

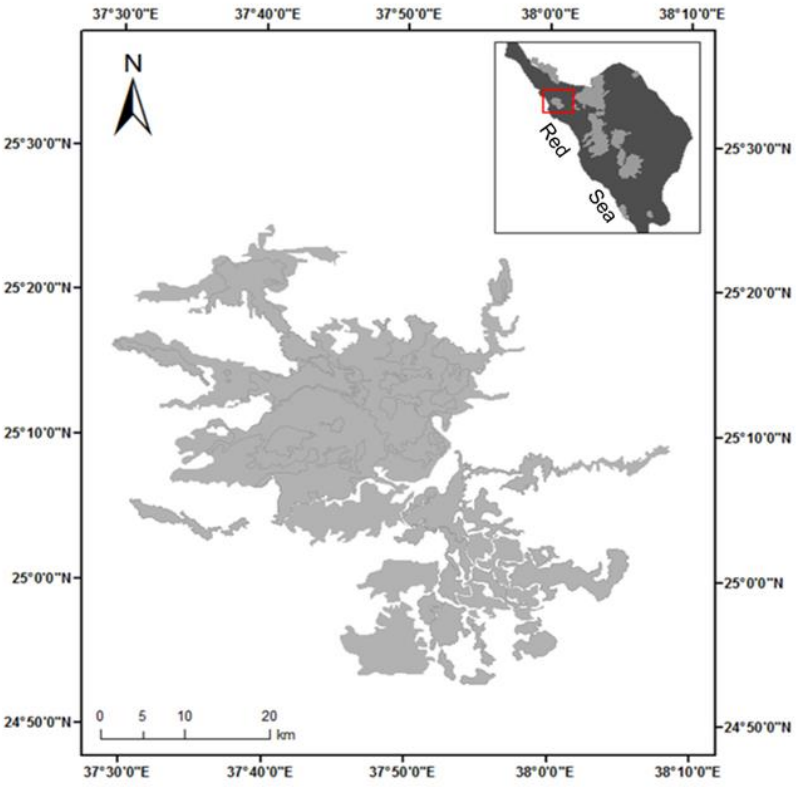

Fig. 2. *Details of the Harrat Lunayyir volcanic field. On the inset, the location of the field within the fields shown in Fig. 1.*

the likely conditions for the 2009 dyke arrest in Harrat Lunayyir and the implications of the results for volcanic hazards. For understanding the 2009 episode, we first provide brief outline of the geological setting of the Harrat Lunayyir, as well as a short overview of its volcanic geology.

2. Regional geological setting

The Harrat Lunayyir forms a part of the Arabian Plate, which is adjacent to the African Plate, with several other plates being nearby (Fig. 1). The eastern part of the Arabian Plate consists of a late Proterozoic shield (Genna et al., 2002) which is bounded to the southwest by the African Plate, the Red Sea rift separating the plates. The other plates in the area are the Eurasian Plate, in the east, and the Anatolian Plate, in the north. The Arabian Plate was generated by the African Rift that led to the formation of the Red Sea and the Gulf of Aden during a rifting episode which began about ~25 Ma ago (Stern and Johnson, 2010).

The Red Sea is considered an active rift zone that emerged from a weakness formed during continental rifting in the pre-Cambrian era (Cochran and Karner, 2007; Bailey, 2009).

Fig. 3. *Volcanic geology of the Harrat Lunayyir volcanic field. a. Basaltic lava flow of Quaternary age (Maqrah basalt). b. Basaltic lava flow of Tertiary age (Jarad basalt). c. An irregularly shaped basaltic dyke, light coloured (people standing on the dyke). d. Volcanic ash partly covering a hill. The thickness of the nearby pahoehoe lava flow is a few tens of centimetres.*

The present rifting led to the expansion and propagation of the Red Sea from the south to the north. Currently, the Red Sea extends from 30° N (the north limit of the Gulf of Suez) to 12.5° N (where it meets the Gulf of Aden), with a total north-south length of about 2,250 km and a maximum east-west width of about 354 km – the oceanic crust itself being of maximum width of about 100 km. The Red Sea may be regarded as an excellent example of the early stages of ocean development through sea-floor spreading. The Gulf of Aqaba-Dead Sea Transform Fault represents another major tectonic element in the area. During spreading of the Red Sea, parts of the Arabian Shield have become extended and thinned (as discussed below) with associated formation of dyke swarms and volcanic fields, one of which is the Harrat Lunayyir (Genna et al.,2002; Hansen et al., 2013).

The Arabian Shield itself occupies one-third of the Arabian Peninsula with an estimate area ranging from 670,000 km^2 to 725,000 km^2 (Brown et al., 1978). The Arabian Shield it is

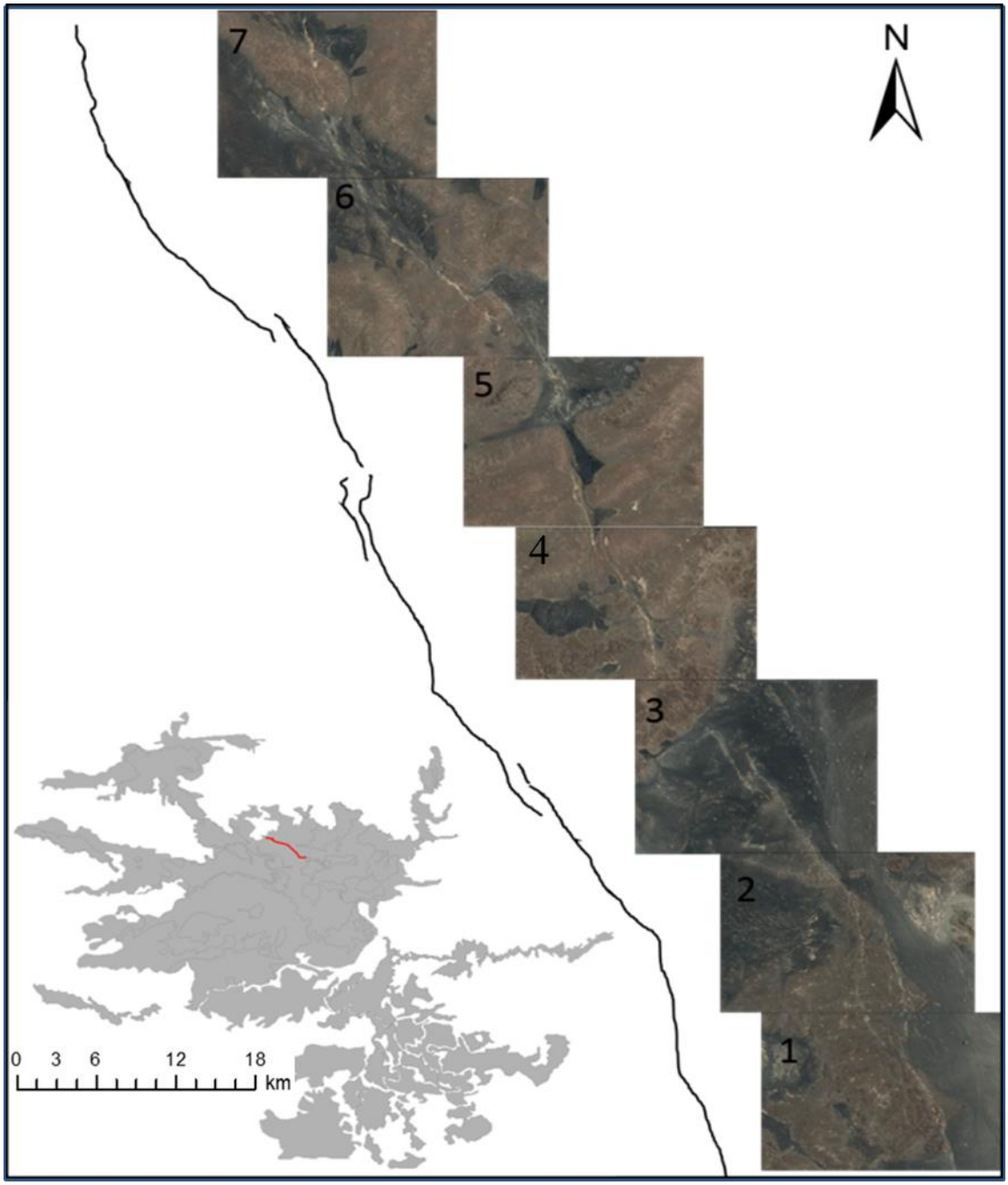

Fig. 4. *Image and sketch of a part of one of the main faults on the western side of the fracture zone/graben formed during the 2009 episode. The total length of the fault part seen here is about 2.5 km. The inset in the left lower corner shows the length of the entire fault and its location within Harrat Lunayyir.*

a part of a larger group referred to as the Arabian-Nubian Shield whose total area is around 2.7×10^6 km^2 (Rodgers et al., 1999; Johnson and Woldehaimanot, 2003). Precambrian crystalline rocks, Phanerozoic sedimentary rocks, and Cenozoic flood basalts (such as at Harrat Lunayyir) constitute the uppermost part of the western part of the Arabian Shield. This is the part that occupies the northeast flank of the Red Sea, including the well-exposed highlands of Yemen and the central part of Saudi Arabia, Najd (Powers et al., 1963; Stern

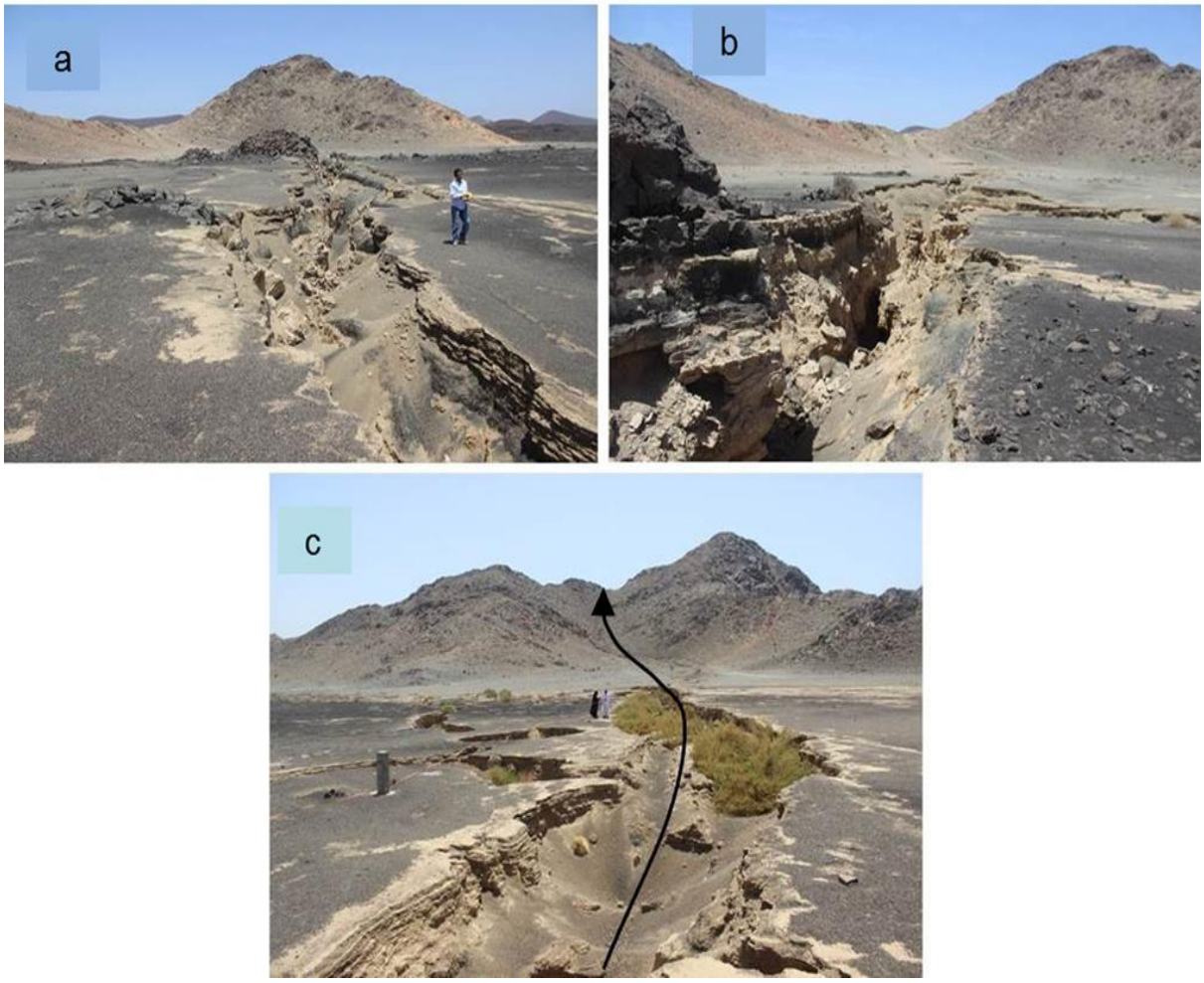

Fig. 5. *Tension fractures at the western side of the fracture zone/graben, generated during the 2009 episode. a. The tension fracture cutting through pyroclastic and sedimentary rocks and lava at the surface, with irregular walls and considerable collapse. The person provides a scale. b. Close-up of part of the tension fracture in a. The maximum opening at the surface is a few metres, but partly due to collapsed walls c. Tension fracture dissecting pyroclastic and sedimentary rocks. The overall strike of the fracture, indicated schematically by an arrow, is north-northwest (cf. Fig. 8). The persons provide a scale.*

and Johnson., 2010) (Fig. 1). The average crustal thickness of the Arabian Shield is about 40 km (Al-Damegh et al., 2005), but the crust becomes thinner towards the coast of the Red Sea where the thickness is 23-25 km. Similar crustal thicknesses occur in the Nubian Shield on the west side of the Red Sea, the thickness being 25-26 km in Egypt within 50 km of the coast of the Red Sea (Hosny and Nyblade, 2014). The crustal thickness in the eastern part of the Arabian Shield is much greater than in the western part (Camp and Roobol, 1992; Stern, 2008). Duncan and Al-Amri (2013).

Close to the volcanic areas of the Arabian Shield is the Afar Triangle, a depression generated by the Afar Triple Junction (Waltham, 2005) where the rift zones of the Red Sea, the Gulf of Aden, and the East African Rift meet (Keir et al., 2012). The crustal spreading is

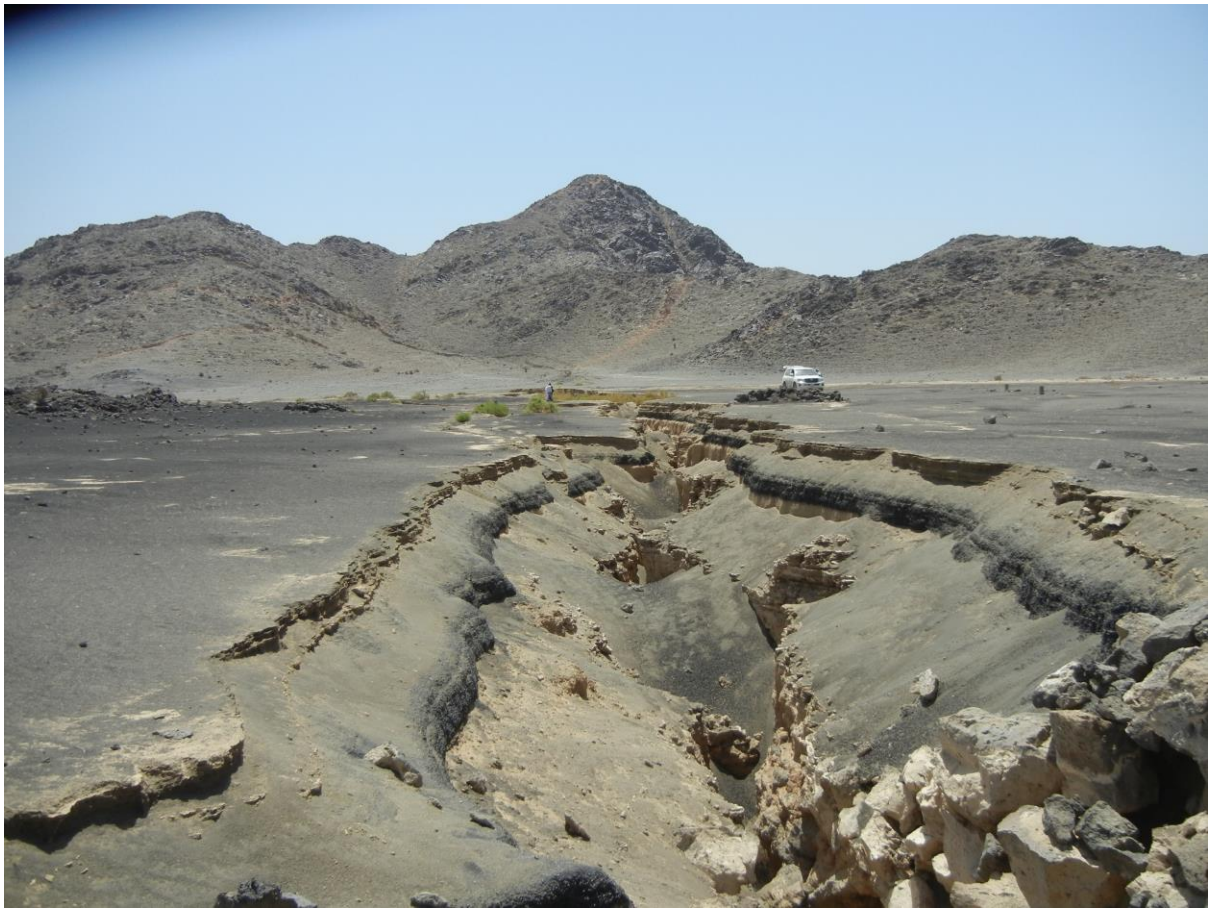

Fig. 6. *Close-up of a northwest-striking tension fracture dissecting pyroclastic and sedimentary rocks at the western side of the fracture zone/graben generated during the 2009 episode. In these compliant layers, there is considerable collapse, so that opening at the surface appears much greater than the real opening (seen in the deepest exposed part of the fracture). The car and the person provide a scale.*

at the rate of 1-2 cm/year across each of the arms or legs of the Triangle. The Triangle is also the site of a hot spot, and widely regarded as the surface expression of a deep mantle plume (Hansen et al., 2013).

3. Volcanic geology of the Harrat Lunayyir

The western part of the Arabian Plate has been volcanically active during the Cenozoic. The activity has been largely confined to two episodes: one happened from 30 to 20 Ma ago while the other began some 12 Ma ago and is still continuing (Roobol et al., 1992). The cumulative area covered by these relatively young volcanic materials is about 80,000 km^2. The lava fields themselves are commonly known as 'Harrats' (Pint, 2006). Harrat Lunayyir (also known as Harrat Al-Shaqa) is one of smallest and youngest of the alkali basaltic Holocene lava fields in western Saudi Arabia. More specifically, the lava field is located northwest of the city of Medina (Al-Madinah Al Munawwarah in Arabic) between latitudes 25° 10` - 25° 17` N and longitudes 37° 45` - 37° 75` E. The lava field is somewhat elongated in the

Fig. 7. *Mixed-mode fracture, an open normal fault, generated during the 2009 episode and dissecting sedimentary rocks at western side of the fracture zone/graben, generated during the 2009 episode. The trace of the fracture is curved, a common geometry of normal faults and tension fractures in mechanically weak rocks. The overall strike is northwest. Where the person is kneeling, the maximum throw is about 0.9 m while the opening is about 0.4 m. The people and the car provide a scale.*

northwest-southeast direction and located about 60 km east of the nearby coast of the Red Sea or, alternatively, some 150 km east of the Red Sea spreading centre (Al-Amri and Fnais, 2009; Baer and Hamiel, 2010; Al-Zahrani et al., 2013; Duncan and Al-Amri, 2013) (Fig. 2).

Harrat Lunayyir is characterised by Cenozoic alkali-olivine-basalt lava flows (Duncan and Al-Amri, 2013) and about 50 monogenetic crater cones (Baer and Hamiel, 2010). The basaltic lava flows in the area have been divided into ‘an older Tertiary unit (Jarad basalt)’ and ‘a younger Quaternary unit (Maqrah basalt)’ by Al-Amri et al. (2012) (Fig. 3). Precambrian rocks are exposed in the northern, southern, and eastern parts of Harrat Lunayyir, while in the central part the Precambrian rocks form only isolated outcrops (Duncan and Al-Amri, 2013). Volcanic activity in Harrat Lunayyir began about 0.5 Ma ago. The youngest lava flows in the field are generally regarded as about 5000 year old (Al-Amri and Al-Mogren, 2011). Eruptions in the area, however, may be more recent, since there is some evidence that one of the crater cones was formed about 1000 years ago (Baer and Hamiel, 2010).

4. The 2007 and 2009 volcanotectonic episodes

Harrat Lunayyir was until recently considered inactive. As indicated above, the last eruption in the area is at least 1000 years old and more likely 5000 years old. However, in October 2007 a volcanotectonic episode began in the area, characterised by an earthquake swarm (Al-Amri and Al-Mogren, 2011; Mukhopadhyay et al., 2013; Zobin et al., 2013). The earthquake swarm was comparatively small, including about 500 earthquakes, the largest one being of moment magnitude M3.2. The swarm came to an end in May 2008. The swarm indicates a source with a northwest-southeast strike and located at depth in excess of 10 km. No surface deformation was associated with this episode (Xu et al., 2016).

Another volcanotectonic episode began 18 April 2009, reached its peak 17-19 May, and came to an end in July the same year (Al-Mahri et al., 2009; Baer and Hamiel, 2010; Pallister et al., 2010; Koulakov et al., 2014; Xu et al., 2016). Again, there was an earthquake swarm with a general northwest-southeast strike, but the swarm was located some 15 km to the northwest of the 2007 swarm. The 2009 swarm generated over 30,000 recorded earthquakes, peaked in its intensity 17-19 May with a sequence of 7 earthquakes of M>4, including the largest earthquake during the episode, of M5.7 (Baer and Hamil, 2010; Xu et al., 2016). The focal mechanisms of the M>4 earthquakes indicate primarily normal faulting, some of which showed evidence of strike-slip components. The main episode came to an end in July 2009. Al-Zahrani et al. (2013) estimate the focal depth of the largest earthquake, M5.7, as 9 km. Most of the earthquakes were located at depths of 5-15 km and have an overall strike of NNW-SSE (Xu et al., 2016).

In addition to the earthquake swarm, there was extensive surface deformation during the 2009 episode (Figs. 4-7). There was, first, a broad area of uplift and extension, the area being about 2000 km^2 with a maximum uplift of about 0.4 m and an extension of about 1 m (Pallister et al., 2010). The total NNW-SSE length of the uplifted area is 14-15 km (cf. Fig. 4). Subsequent studies suggest a total extension of about 1.5 m across the deformation zone, and a subsidence of a maximum of 0.8 m in the central part of a ‘graben’ that dissects the dome (Baer and Hamel, 2010). Doming normally generates tensile and shear stresses in the surface layers, as is well known from analytical models (e.g., Gudmundsson, 1987, 1999), and the same applies to general spreading (e.g., Gudmundsson, 2017). These stresses, in turn, may reach the tensile or shear strength of the rocks so as to generate tension fractures and/or normal faults. While regional doming, possibly combined with general spreading, very likely contributed to the observed fracture formation during and prior to the 2009 episode, the focus here is on the dyke-induced stresses and fracture formation. As indicated above, the particular aim is to understand how much of the fracture pattern could have been generated by dyke-induced stresses and how deep the dyke tip would have to be to generate the fractures. Following the established tradition, we use the word ‘graben’ for the general surface deformation of the 2009 episode. Later in the paper, however, we discuss in which way, if any, the actual deformation can be regarded as a classical graben structure.

4.1 Surface fractures

In addition to the uplift and general extension, there was considerable fracture development, particularly close to the centre of the uplift or dome. The fractures are of two main types:

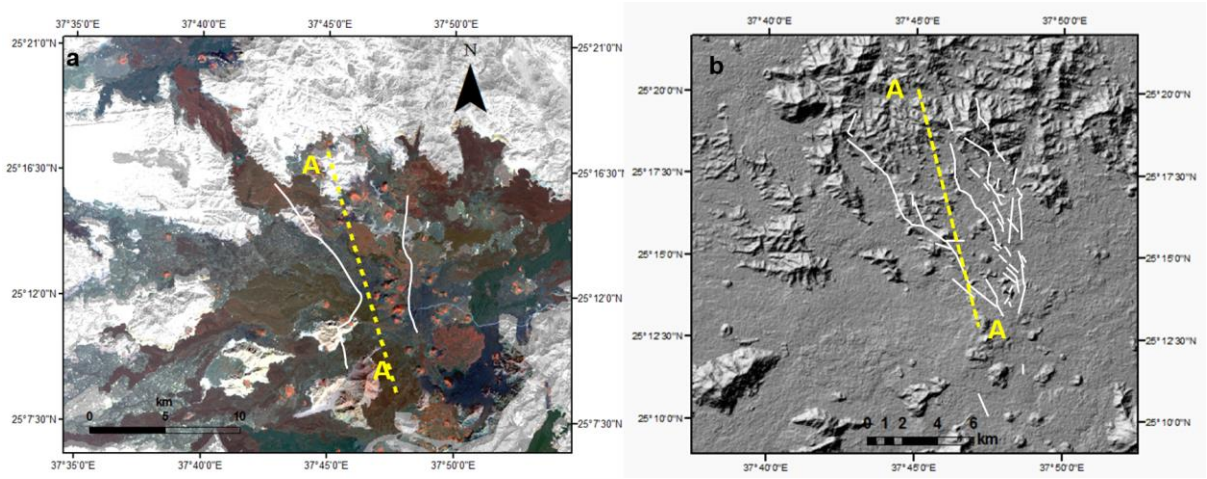

Fig. 8. *Main fractures generated or reactivated during the 2009 episode in relation to the projected strike and strike dimension (length) of the associated dyke. a. The principal active/new fractures during the 2009 episode in relation to the surface projection of the inferred dyke, broken line A to A', and the lava field of Harrat Lunayyir. Notice the difference in strike between the dyke and the fractures, particularly the main fractures (tension fractures and normal faults) at the western margin of the fracture zone/graben. b. Detailed map of the fracture pattern generated during the 2009 episode. Notice the variety in fracture strike in comparison with the inferred dyke strike and the broad system of (tension) fractures at the eastern side of the fracture zone/graben. In this interpretation, the projection of the dyke dissects some of the fractures at the western side of the fracture zone/graben. Data from Baer and Hamil (2010).*

tension fractures (Figs. 5-6) and normal faults (Fig. 7). The tension fractures and normal faults that formed or became reactivated during the volcanotectonic episode reach cumulative lengths of up to 8 km (Figs. 4-6; cf. Baer and Hamiel, 2010; Pallister et al., 2010). While the rupture was still clearly seen during our field studies in 2015 and 2016, in the sedimentary and tephra layers subsequent collapses and erosion make it difficult to estimate the openings accurately (Figs. 5-7). The field data, however, show that many of the fractures that constitute the rupture zone are pure tension fractures rather than normal faults (Figs. 5-6). Normal-fault displacement was, however, seen on some of the fractures (Fig. 7). The most accurately measured displacement measured in the field was made during the episode (in June 2009) by Pallister et al. (2010) where they measured a normal fault along part of its 8-km-long surface rupture. Their results show an open or gaping normal fault with a vertical displacement or throw of 0.78 m and opening (aperture) of 0.45 m. The fault wall is vertical (Fig. 7). This fault is thus clearly a mixed-mode (mode I and mode II) fault formed at the surface in absolute tension – similar to numerous mixed-mode fractures in the pahoehoe lava flows in the rift zone of Iceland (Gudmundsson, 2017). Other throw measurements at the western boundary of the area (graben) yield 0.6 m, whereas pure tension fractures at the eastern boundary show openings (apertures) of tens of centimetres (Jonsson, 2012). The tensional axes inferred from focal mechanism during the episode strike mostly ENE-WSW

Fig. 9. *Basaltic dyke arrested in a vertical section in Tenerife (Canary Islands). The host rock by comparatively soft (compliant) pyroclastic rock. The dyke becomes arrested at its contact with much stiffer (higher Young's modulus) inclined sheet, as forecasted by the elastic mismatch mechanism of dyke arrest. The maximum thickness of the dyke is about 0.8 m. There are no dyke-induced extension fractures or faults at the tip. The person provides a scale.*

Fig. 10. *Subvertical basaltic dyke arrested in a vertical section in Tenerife. The main host rock is a pyroclastic layer (red-pink) on top of which is a basaltic lava flow (black-blue). The dyke becomes arrested roughly at the contact between the pyroclastic layer and the lava flow. More specifically, on meeting the contact, the dyke abruptly becomes much thinner (its maximum thickness is 0.26 m at the bottom of the 3.7 m tall exposure) and tapers away to its tip. The length of the yellow steel tape parallel with the lowermost right margin of the dyke is 1 m. There are no dyke-induced extension fractures or faults at the tip. The arrest mechanism here is most likely a stress barrier.*

(Pallister et al., 2010) and thus roughly perpendicular to the tension fractures and open normal faults seen in the field (Figs. 4-7).

Our fracture studies focused primarily on the western part of the graben. What is most noticeable in the parts that we studied are large tension fractures (Figs. 5-6). While these have collapsed since their formation, it is clear from the deeper parts that the openings range from tens of centimetres to about one metre (Fig. 6). The fracture walls on either side are at the same elevation, which shows that there is no normal-fault component in these fractures, and there is also no evidence of strike-slip. The fractures are thus pure tension fractures or mode I cracks. We observed numerous tension fractures along the western side of the graben, but also some normal faults (Fig. 7). Jonsson (2012) confirmed that during the earthquake swarm the fractures formed on the eastern side of the graben were primarily tension fractures.

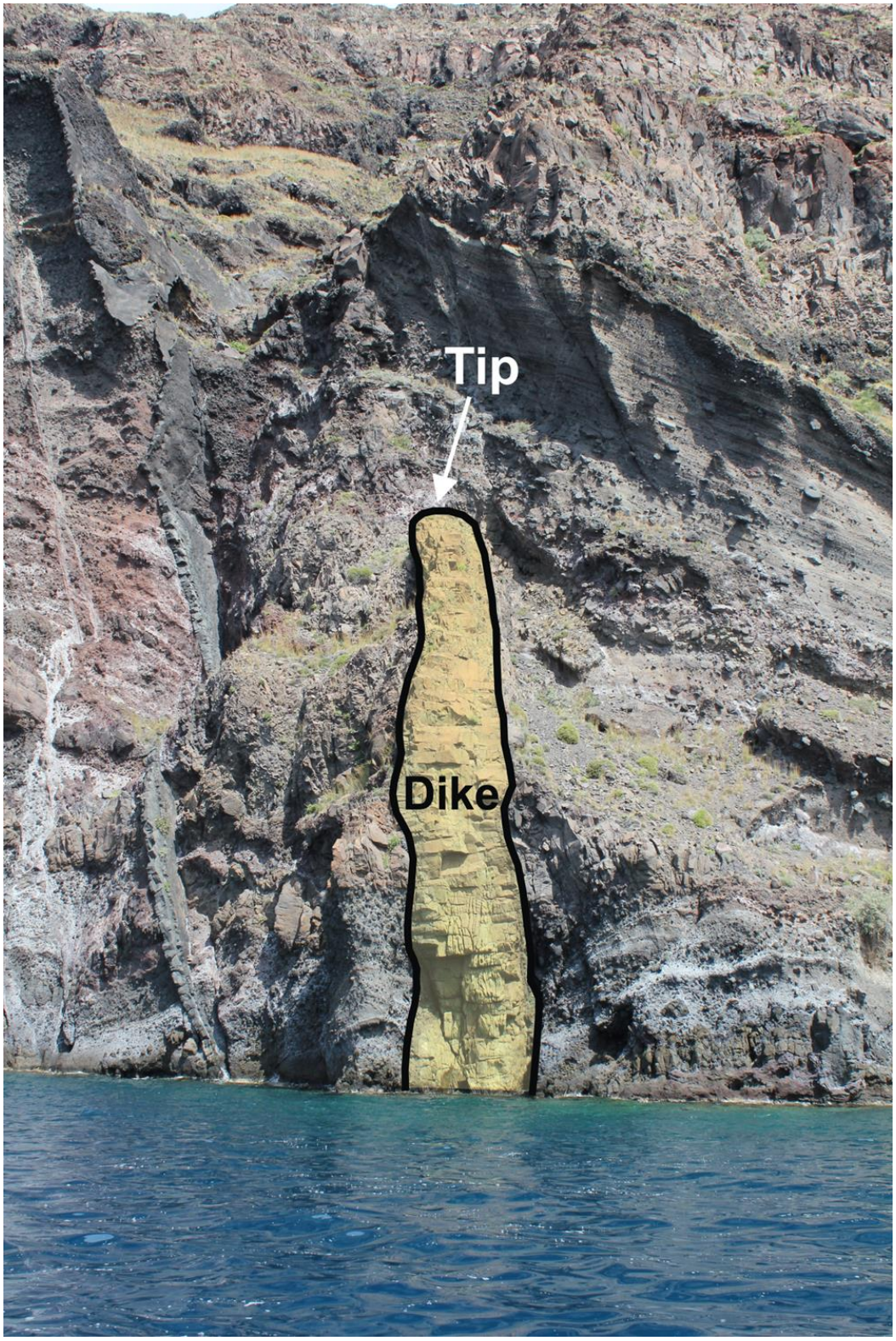

Fig. 11. *Arrested dyke in the caldera wall of Santorini (Greece). The dyke is arrested at the contact between layers of pyroclastic rock. The grain size of the layers changes abruptly at the contact, and thereby their mechanical properties. The maximum dyke thickness at sea level is about 2 m. The arrest mechanism here is most likely elastic mismatch.*

All the observations of surface fracturing during the 2009 volcanotectonic eposide thus show that tension fractures were the most common, but that there were also some small normal faults. The normal faults were mostly confined to the western side of the graben whereas tension fractures formed both on the western and eastern sides. The surface deformation, however, was not confined to the graben boundaries since many fractures formed inside the graben (Fig. 8).

Clearly, the detailed fracture pattern in Fig. 8a does not show a great resemblance to that in Fig. 8b. In Fig. 8a the white lines show the 'InSAR-determined faults', whereas the fracture pattern in Fig. 8b was derived from 'differential coherence maps', with black lines showing incoherent lineaments for the entire rifting episode and white lines for the period 27 May to 1 July 2009 (Baer and Hamiel, 2010). In Fig. 8a there are two main sets of fractures: a set of NW-striking fractures found at both sides of the graben, and then a set of roughly N-striking fractures, found primarily at the eastern side of the graben – although one such fracture occurs at the north end of the fracture set at the western side of the graben. The overall strike of the NW-set along the western side is roughly 315° whereas the common general strike of the N-striking fractures on the eastern side is about 352°. Thus, the angle between the two sets is about 37°. However, when individual fractures shown on Fig. 8b are measured, they range in strike from about 305° (northwest) to about 25° (north-northeast), yielding a maximum acute angle between the fractures of some 80°. Since the fractures are all thought to have formed during the 2009 episode, it is clear that they must have been subject to widely different local stresses, part of which may relate to the inferred dyke emplacement during the episode.

4.2 Comparison of earthquake swarms in 2007 and 2009

The general interpretation of the 2009 earthquake swarm is that it was, partly at least, triggered by dyke propagation (Baer and Hamiel, 2010; Pallister et al., 2010; Hansen et al., 2013; Xu et al., 2016). While no earthquake migration was observed, the interpretation that at least part of the swarm was associated with a dyke that failed to reach the surface – that is, became arrested – is plausible and one that we take as a basis for our analysis.

We interpret the data provided in the cited papers as follows:

- The seismic swarm in October 2007 may be seen as a precursor to the main swarm associated with subsequent dyke emplacement in April-July 2009. We interpret the precursor so that a deep-seated reservoir was subject to inflation and possibly rupture. During inflation of a reservoir, reactivation of fractures, particularly faults, in its roof would normally generate earthquakes.
- There are, however, remarkable differences between the October 2007 swarm and the April-July 2009 swarm. These differences include a different location (including depth), number of earthquakes, and surface effects. (a) The October 2007 swarm generated only about 500 recorded earthquakes and was mostly some 15 km to the southeast of the April-July 2009 swarm which generated about 30,000 recorded earthquakes. (b) The October 2007 swarm was generally much deeper than the April-July 2009 swarm. In particular, the earthquakes of the October 2007 swarm were mostly located deeper than about 10 km, and many reached depths of 25-30 km. (c)

By contrast, although the deepest earthquakes of the April-July 2009 swarm reach depths of 25-30 km, the great majority of the earthquakes are shallower than 20 km, and very many occurred at depths between 10 km and the surface. (d) In contrast to the April-July 2009 swarm, there was no recorded surface deformation during the October 2007 swarm.

- There are also certain similarities between the swarms. One is that they occur in basically the same area, even if not at the same location. Another is that both can be interpreted as being partly associated with apparently steep-dipping structures (between about 55° and 65°) to the east (Xu et al., 2016, fig. 2). However, for both swarms this apparent dip may be an illusion because of the way the earthquakes concentrate in certain layers. In case of the October 2007 swarm, the dip can, in fact, be interpreted in various ways, and there is clear concentration of earthquakes at depths of about 10-15 km, 20-24 km, and 27-30 km. As for the April-July 2009 swarm, similar concentrations of earthquakes occur at depths of 2-8 km (although many earthquakes reach the surface), and 12-17 km (although some earthquakes occur at depths of 20-30 km).
- The concentration of earthquakes at certain depth intervals in the crust is very common and relates normally to stiff (high-Young's modulus) units or layers. Thus, during loading of the crust, the stiff units or layers concentrate much more stress (either in tension or compression) than the more compliant or softer layers. The lateral spread in earthquakes in the uppermost part of the crust during the April-July 2009 episode and 10-15 km and 27-30 km depth in the October 2007 episode may thus be attributable to the crustal layers or units at these depths being stiffer than adjacent units. Another interpretation is that some of the laterally spread earthquakes may be located in the roof of a magma reservoir – as is commonly observed during unrest and dyke injections (e.g., Becerril et al., 2013). But in the present cases, neither swarm has a distribution in space that is easily interpreted as roof failure due to magma-pressure changes (inflation) of a reservoir. We therefore think it is more likely that many of the earthquakes, particularly in the April-July 2009 swarm, relate to dyke emplacement.

4.3 Dyke emplacement

The data on the October 2007 swarm are too limited to allow us to decide whether or not there was any dyke emplacement. But contrast, the data, presented above and below, suggests that there was dyke emplacement during the April-July 2009 earthquake swarm. The focus here is on the 2009 swarm.

A swarm of earthquakes of this kind is typically associated with dyke emplacement. It is then the magmatic pressure within the dyke that triggers many of the fault-slips that generate the earthquakes. Focal mechanisms of the larger events (M>4) indicate mostly normal faulting with some strike-slip components. This is in contrast to the earthquakes generated during the dyke emplacement in Bardarbunga in Iceland 2014 where most of the earthquakes were strike-slip (Agustsdottir et al., 2016). Strike-slip and some reverse slip (Gudmundsson et al., 2008) are expected in the walls of a dyke, since they become subject to horizontal

Fig. 12. *Arrested basaltic dyke in the lava pile of East Iceland. At the base of the photograph the dyke is about 2 m thick, but gradually thins towards its tip. The host rock is basaltic lava flows with scoria and soil layers (red) in-between. The arrest mechanism here is most likely a stress barrier, located in the layers above the tip of the dyke. On meeting a stress barrier, a dyke commonly thins before either stopping its propagation altogether (as here) or deflecting into a sill.*

compressive stress due to the magmatic overpressure of the dyke, which in turn induces shear stresses on some of the existing fractures, particularly joints. Since many of the earthquakes during the 2009 swarm, by contrast, seem to be associated with normal faulting, this may indicate two basic processes:

a. Much of the faulting may occur ahead of an upward-propagating dyke tip. In the 'process zone' around the dyke tip extension fracturing and normal faulting is common (Gudmundsson, 2011a). In this zone, normal-fault earthquakes are commonly generated by slips on existing fractures, many of which are cooling joints in the lava pile. Some dykes also use existing, steeply dipping normal faults as parts of their paths, in which case slip on an existing normal fault would be facilitated by the dyke-magma entering the fault plane (Gudmundsson, 2011a). The macroscopic dyke-fracture itself, however, is primarily an extension fracture (mode I crack) and thus does not generate classical double-couple earthquakes.

b. Part of the fault slip may be generated on existing normal faults, presumably buried by younger layers before the 2009 episode and thus not seen earlier in the field or on aerial photographs. When the earthquake swarm is used to infer the dip – irrespective of the points discussed above as to concentration of earthquake in particular layers or units – then the overall dip would be about 65°E. It is possible that many of the earthquakes were associated with the western boundary faults of the graben. However, in case slip on the fault was triggered by the magmatic overpressure of the dyke, one would rather expect strike-slip or reverse faulting on the main boundary fault, as is commonly inferred and observed where dyke enter existing grabens (Gudmundsson and Loetveit, 2005; Gudmundsson et al., 2008).

Normal faulting and dyke emplacement are the most common large-scale processes associated with rifting worldwide. This is understandable since both are attributable to extension, that is, to the relative tension which dominates in rift zones. The processes may operate simultaneously; that is to say, dyke injection and normal faulting may both occur without necessarily one triggering the other. Normal faulting is common without dyke emplacement, such as in sedimentary basins, and most dykes become arrested without generating any large-scale normal faults or grabens. In fact, field studies in Iceland show clearly that where normal faults are common in parts of palaeo-rift zones, dykes are comparatively rare, and vice versa (Forslund and Gudmundsson, 1991). This is because there is essentially constant spreading rate in rift zones, so that if much of the spreading is accommodated by normal faulting then less will be accommodated by dykes, and vice versa. The general rule is, however, that the contribution of dykes to the overall spreading at plate boundaries everywhere varies positively with increasing crustal depth (e.g., Gudmundsson, 2002).

As indicated above, one of the unsolved issues with the 2009 episode is whether or not the inferred dip of the earthquake swarm is real or an artefact. We have already explained how it may be an artefact due to stress concentrations in layers and units of different stiffness. If, however, the dip is real and about 65°, then we should be able to relate the dip to the two main processes discussed above. For the second process, there is no problem in doing so since a dip of about 65° is a common dip of normal faults in continental areas.

For the first process, however, we would have to explain why the dyke triggering much of the normal faulting did not follow a vertical path but rather path dipping 65°. For a magma reservoir of either a sill-like or dome-like geometry, as appear to be the most common shapes (Gudmundsson, 2012, 2017), horizontal tension related to rifting would normally result in subvertical trajectories of the maximum principal compressive stress, σ_1. As is well known, dyke propagation paths tend to follow the trajectories of σ_1 and, thereby, being perpendicular to the trajectories of the minimum compressive (maximum tensile) principal stress, σ_3. However, if the main loading is internal magmatic excess pressure, then the trajectories of σ_1 become generally curved away from the reservoir, and may dip by as much as 65°, particularly above and beyond the marginal parts of the reservoir (Gudmundsson, 2002).

It is thus possible to explain the dip of the 2009 earthquake swarm in various ways. Not only as a result of crustal layering and variation in local stresses – which may certainly play a role and contribute to the dip being, partly at least, and artefact – but also as a direct

consequence of either a major normal fault (the western boundary fault of the graben) or a dyke injected from the marginal parts of the source reservoir whose loading is then primarily internal magmatic excess pressure. In what follows, we assume that the earthquake swarm was largely, or primarily, the result of dyke injection and propagation towards the surface. The focus in the models is on understanding better the potential surface effects of such a dyke and trying to estimate as well as may be the likely depth of the tip of the dyke at the time of arrest. This latter is of very great importance when assessing the hazard in the area, and has implications for hazard and risk assessments in volcanic areas in general.

5. Dyke arrest

Most dykes become arrested. Hundreds of arrested dykes have been observed, and many tips of such dykes studied in detail. Field studies show that while some dykes terminate within layers, most dykes become arrested at contacts between rock layers or units; in particular, at contacts between mechanically dissimilar layers (Figs. 9-12; Gudmundsson, 2002, 2003). Some of these dykes become deflected into sills (e.g. Tibaldi and Pasquare, 2008; Casagli et al., 2009; Gudmundsson, 2011b; Barnett and Gudmundsson, 2014; Tibaldi, 2015), whereas others become arrested on meeting the contact (Figs. 9-12).

There are three principal mechanisms by which dykes (and other extension fractures or mode I cracks) become arrested: (1) Gook-Cordon delamination, (2) stress barrier, and (3) elastic mismatch. All the mechanisms may operate simultaneously, but the Gook-Cordon delamination is most effective at shallow crustal depths. The other two mechanisms can operate at any depth. A detailed description of these mechanisms, including appropriate references, is given by Gudmundsson (2011a,b), so only a brief discussion is provided here.

The Cook-Gordon delamination mechanism implies that the contact that arrests the dyke is mechanically weak. By this we mean that the tensile strength (and, by implication, the shear strength also, because these are related) is low. Around the dyke tip there is a tensile stress field. The highest tensile stress is orientated dyke-perpendicular, and operates to generate the dyke fracture. But there is also a high dyke-parallel tensile stress which, for a contact with a low tensile strength, may open up the contact when the dyke tip is close to it. Opening of a contact is observed in many numerical models of dyke emplacement (Gudmundsson, 2003, 2011a) and is likely to occur in nature. When the dyke tip finally reaches the open contact, the tip then becomes either deflected along the contact to form sill or, alternatively, stops altogether, that is, becomes arrested.

Stress barrier is a layer or unit where the local stress field is unfavourable for a particular type of fracture propagation. For a vertical dyke, a stress barrier is a layer/unit where the compressive stress perpendicular to the projection of the dyke path/plane up into the layer/unit is either the maximum or the intermediate principal compressive stress, that is, σ_1 or σ_2, both being compressive. Since a dyke is an extension fracture, a mode I crack, it propagates along a path whose direction is parallel with σ_1 and σ_2 and perpendicular to the minimum compressive (maximum tensile) principal stress σ_3. Thus, once a vertical dyke tip approaches and tries to enter a layer where σ_1 and σ_2 are horizontal and σ_3 thus vertical, the dyke must either deflect into a sill or become arrested altogether. Stress barriers form in various ways, but perhaps the most common in volcanic rift zones is that earlier dyke

injections have resulted in a 90° flip of the principal stresses because of their magmatic overpressure which compresses the surrounding rock horizontally.. For example, consider a dyke with an overpressure of 15 MPa propagating through a layer where, originally, the principal stresses are σ_1 = 50 MPa, σ_2 = 45 MPa, and σ_3 = 40 MPa. Following the dyke emplacement the horizontal stress close to the dyke, initially σ_3 = 40 MPa, becomes 40 + 15 = 55 MPa, and thus the largest compressive stress, that is, σ_1. Thereby, the layer, temporarily, becomes a stress barriers to subsequent vertical dyke propagation. Given that the crustal segment hosting the layer constitutes a part of a rift zone, the high horizontal stress of 55 MPa is eventually relaxed (through spreading) and the state of stress flips back to the original. Slip on the boundary faults of a graben may also generate stress barriers to dyke propagation (Gudmundsson, 2011a).

Elastic mismatch is a name given to the mechanism where deflection and arrest are primarily controlled by the contrast – the mismatch – in elastic properties of the layers on either side of a contact, in relation to the elastic properties of the contact itself (He and Hutchinson, 1989; Hutchinson, 1996; cf. Gudmundsson 2011a,b) . More specifically, the probability of a dyke becoming deflected into a sill or arrested at a contact is related to the Dundurs elastic extensional mismatch parameter α_D (He and Hutchinson, 1989; Hutchinson, 1996):

$$\alpha_D = \frac{E_1 - E_2}{E_1 + E_2} \tag{1}$$

where E is the plane-strain extensional Young's modulus (stiffness). Arrest or deflection of a dyke, or an extension (mode I) fracture in general, on meeting a contact is encouraged when the Young's modulus of the layer hosting the fracture (E_2) and below the contact is lower than that of the layer above the contact (E_1). The probability of dyke arrest at a contact varies positively with increasing elastic mismatch or difference between E_1 and E_2, that is, with increasing Dundurs parameter (Gudmundsson, 2011a,b). More specifically, arrest of a dyke or its deflection into a sill is more likely when the layer above the contact (E_1 has a higher Young's modulus than the layer below the contact (E_2).

While field observations show that most dykes are arrested at layer contacts (Figs. 9-11) and other discontinuities such as faults, some dyke simply taper away in layers presumably where the overpressure gradually decreases. Commonly, this happens when the dyke tip approaches a contact where the stress field is unfavourable; for example, a contact with a layer that acts as a stress barrier (Fig. 12). Part of the reason for dykes tapering away in vertical sections is decrease in magmatic overpressure or driving pressure for a dyke propagating through rocks of an average density less than that of the dyke magma. This is particularly the case for basaltic dykes propagating through low-density pyroclastic and sedimentary rocks. The decrease in magmatic overpressure is then due to negative buoyancy.

Magmatic overpressure in a dyke is given by (Gudmundsson, 2011a):

$$p_o = p_e + (\rho_r - \rho_m)gh + \sigma_d \tag{2}$$

where ρ_r is the average host-rock density, ρ_m is the average magma density, g is acceleration due to gravity, h is the dip dimension of the dyke, and σ_d is the differential stress (the difference between the maximum (σ_1) and the minimum (σ_3) principal stress) in the host rock where the dyke is studied. The second term on the right-hand side of Eq. (5.5) is the buoyancy term. In the uppermost 1-3 km of the crust in almost all volcanic areas, the average rock density is 2500-2600 kg m^{-3} whereas a basaltic magma may have density between 2650 and 2800 kg m^{-3}. It follows that, in the uppermost part of the crust, buoyancy for basaltic magmas is commonly potentially negative. During ascent of magma, there is normally gas expansion which makes the magma lighter, that is, of less density. While gas expansion and density reduction is common in acid magma to depths of many kilometres (Gonnermann and Manga, 2013), much of the gas exsolution in basaltic magma takes place at very shallow depths. In Hawaii, for example, gas exsolution in basaltic magmas occurs primarily in the uppermost few hundred metres of the feeder/conduit (Greenland et al., 1985, 1988). Similarly, direct observations of dykes, sills, and inclined sheets in deeply eroded lava piles and central volcanoes show only small and rather infrequent vesicles (formed by expanding gas) at depths exceeding several hundred below the original surface of the volcanic zone/central volcano. Some feeder-dykes, by contrast, contain large vesicles close to the surface (Galindo and Gudmundsson, 2012).

Thus, density decrease of basaltic magma due to gas exsolution is most likely to occur very close to the surface, mostly in feeder-dykes, and does thus normally not much affect the potential negative buoyancy term in Eq. (2). It follows that, commonly, for basaltic dykes injected from shallow magma chambers, the only driving pressure in Eq. (2) is the excess pressure p_e in the chamber. That pressure is roughly equal to the tensile strength of the walls or, normally, the roof of the magma chamber. The tensile strength of most rocks is between 0.5 and 9 MPa, the most common values being 2-4 MPa. Thus, the excess pressure at the time of magma-chamber rupture and dyke injection may, depending on the variation in tensile strength, vary by a factor of 2-3, and very rarely by a factor of 6-9.

When the only driving pressure of basaltic dykes injected from many shallow magma chambers is the excess pressure, of the order of mega-pascals, the driving pressure or overpressure gradually decreases as the dyke propagates towards the surface. The decrease in overpressure is then partly because of decline in the excess pressure in the source chamber as magma flows out of it and up the dyke. This decline may be described as follows (Gudmundsson, 2016):

$$p(t) = p_e\left(1 - e^{-(\frac{V_{er}}{Qt} - 1)}\right) \qquad (3)$$

where $p(t)$ is the excess-pressure variation in the magma chamber as a function of time, p_e is, as before, the excess pressure at the time of magma-chamber rupture and dyke injection (roughly equal to the in-situ tensile strength), V_{er} is the dyke volume (or, in case of an eruption, the combined dyke and eruptive volume), and Qt is the magma volume (in m^3) that flows out of the chamber during the time interval t. Clearly, the exponent has the units of

m^3/m^3 and is thus dimensionless. Eq. (3) indicates an exponential decrease in excess pressure in the source chamber during the eruption and/or dyke injection until the excess pressure approaches zero, that is, $p(t) \rightarrow 0$, when the bottom of the feeder closes, and the magma flow out of the chamber comes to an end.

A dyke injected from a shallow magma chamber under a very low excess magmatic pressure, say 1 MPa, and propagating through low-density crustal rocks may thus stop on its propagation path simply because the overpressure declines to zero. This would apply primarily if the magma chamber is (a) comparatively small, say with a volume of 20-30 km^3 or less and (b) very shallow, say with a roof at a depth of 1-2 km. Many dykes and, in particular, inclined sheets are seen to taper away in dense sheet swarms associated with such shallow chambers in Iceland and in ophiolites (e.g., Gudmundsson, 2002).

Several other mechanisms suggested for dyke arrest are, based on field observations and theoretical studies, likely to be of minor importance. Thus, it has been suggested that down-bending of the crustal segment on which a volcanic edifice rests generates local stresses that may arrest dykes (Rivalta et al., 2015). There is plenty of evidence of down-bending or sagging of crustal layers in the volcanic zones of Iceland, below volcanic edifices and in the volcanic zones in general, with no known effects as to dyke arrest. Similarly, down-bending of the lithosphere below large volcanic edifices such as in Hawaii has no known effects as to dyke arrest. If down-bending of crustal layers due to piling up of new eruptive material was a major factor in arresting dykes, then no large edifices could form in the first place. Generally, volcano spreading and divergent-plate boundary spreading counters any such effects and the magma chambers stay in close to lithostatic equilibrium with the host rock through most of their lifetimes (except during unrest periods). An edifice takes thousands or tens of thousands of years to form, and the potential down-bending due to the load of each lava flow/pyroclastic layer is normally so small as to have, to hardly any stress effects that could result in dyke arrest.

Similarly, it is commonly suggested that cooling or solidification of the dyke results in its arrest (e.g. Rivalta et al., 2015). However, for dykes injected from shallow magma chambers the rate of propagation is commonly 0.1-1 m s^{-1} and they would normally reach the surface, in case they were feeders, before any significant cooling would take place. Furthermore, even if solidification of the dyke tip would occur – as, for example, if the tip would meet significant amount of groundwater – the solidified tip has the same tensile strength, or slightly lower, than that of the host rock. Thus, so long as there is any magmatic overpressure in the dyke, a temporarily solidified tip should not stop the propagation any more than the host rock would.

Based on the considerations above, we conclude that dyke arrest is primarily controlled by mechanical layering and local stresses along the potential path of the dyke. Given that the 2009 dyke at Harrat Lunayyir most likely generated tension fractures at the surface, and yet became arrested, mechanical layering is the most likely explanation for the dyke's arrest. Which brings us to the surface deformation associated with the dyke emplacement, in particular the formation and depth of the tension fractures.

6. Tension fractures and normal faults

The surface deformation associated with the 2009 dyke emplacement is primarily reflected in the formation or reactivation of tension fractures and normal faults (Figs. 4-8). Tension fractures can only reach a certain depth; if they try to propagate to greater depths they must change into normal faults. This theoretical result follows from Griffith's crack theory, and is supported by actual field observations in active rift zones and fossil rift zones (Gudmundsson, 2011a, 2017).

The two-dimensional Griffith criterion for fracture initiation in the tensile regime is given by:

$$\text{If } \sigma_1 < -3\sigma_3 \text{ then } \sigma_3 = -T_0 \quad (4)$$

Here, σ_1 is the maximum principal compressive stress, σ_3 is the minimum principal compressive stress, and T_0 is the tensile strength of the host rock. On substituting $-T_0$ for σ_3 in the inequality (4), we obtain:

$$\sigma_1 - \sigma_3 < 4T_0 \quad (5)$$

It follows from inequality (5) that the stress difference for the failure criterion in the tensile regime to apply cannot exceed $4T_0$. Using the following equation:

$$\sigma_1 = \rho_r g d \quad (6)$$

where ρ_r is the host-rock density, g is the acceleration due to gravity, and *d* is the fracture depth (dip dimension), the maximum depth d_{max} that a large-scale tension fracture can reach (by definition, in the absence of internal fluid overpressure) is

$$d_{\max} = \frac{3T_0}{\rho_r g} \quad (7)$$

If the tension fracture propagates to greater depth than given by Eq. (7), it must change into a normal fault.

As an example, if the average density of the uppermost part of the crust of 2500 kg m^{-3}, as is common in continental areas, the maximum depth of the tension fractures in Figs. 4 and 5 (other tension fractures are shown by Jonsson, 2012) ranges between about 60 m (for the lowest possible in-situ tensile strength of 0.5 MPa) and 1100 m (for the highest possible tensile strength of 9 MPa). These are extreme tensile-strength values, however. Most commonly, the in-situ tensile strengths of rocks, based on direct measurements through hydraulic fracturing, are 2-3 MPa (Gudmundsson, 2011a). These values are also similar to those obtained by theoretical strain considerations for the rocks in the present area, namely 1-3 MPa, by Jonsson (2012). Thus, using 2-3 MPa as the tensile strength, the most likely maximum depths of the tension fractures in the area would be between 244 and 367 m.

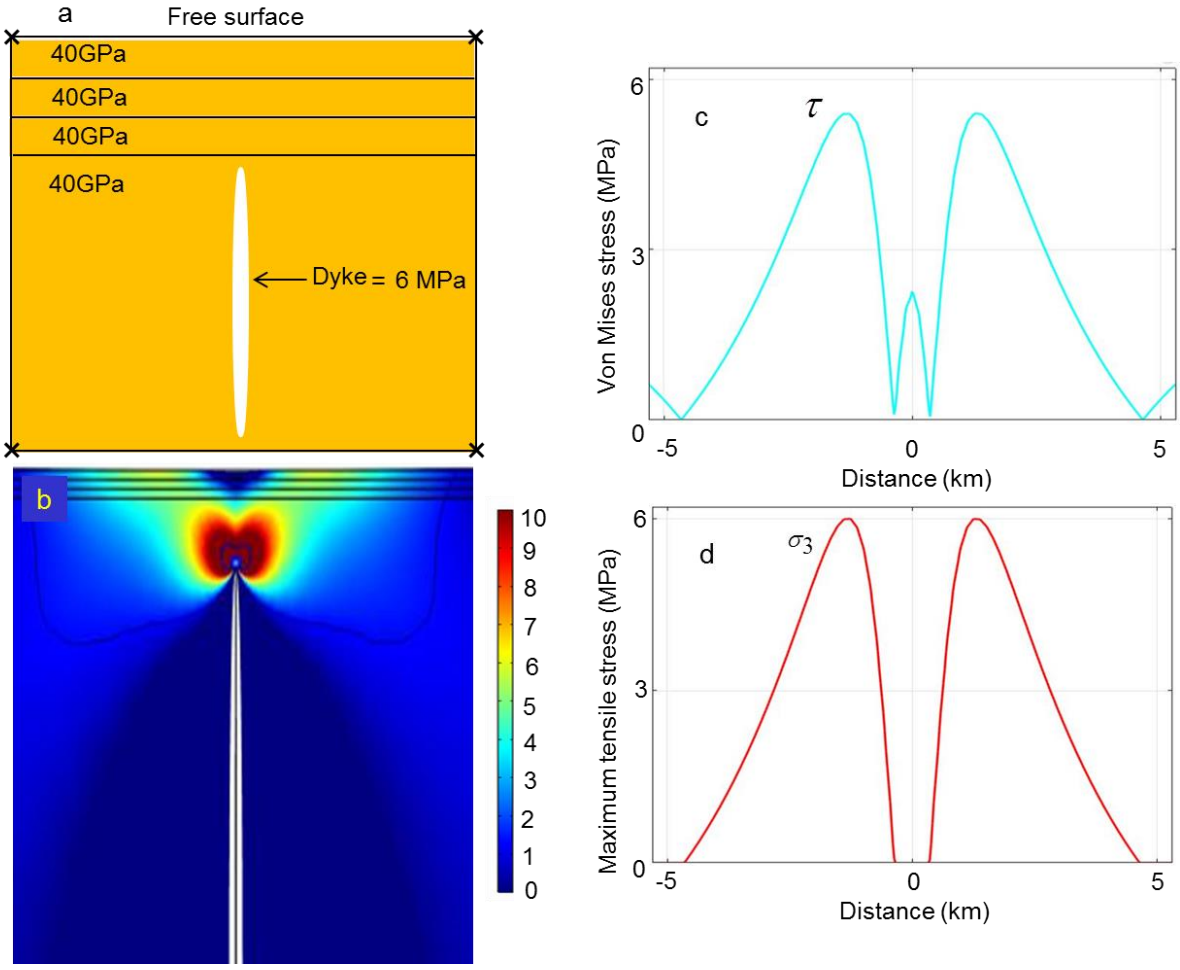

Fig. 13. *Numerical model of a dyke arrested with a tip at the depth of 1000 m below the Earth's surface. The magmatic overpressure is 6 MPa and Poisson's ratio of all the rock layers is 0.25. Each of the 3 top layers is 100 m thick. All the 3 top layers, as well as the main rock unit hosting the dyke have the same Young's modulus of 40 GPa. Thus, this is effectively an elastic half-space model. a. Schematic setup of the model. The thickness of the layers and the height of the dyke are not to scale. b. Maximum principal tensile stress, σ_3, in mega-pascals. The stresses shown here, and in subsequent models, range from 0 (blue) to 10 MPa (red). This range (0-10 MPa) is chosen so because the maximum in-situ tensile strength of crustal rocks is 9 MPa, and mostly 5-6 MPa, so that tensile stresses above 10 MPa can normally not be reached in the crust (Gudmundsson, 2011a). The dip dimension (height) of the dike in all the models is between 9 and 10 km. c. von Mises shear stress at the Earth's surface. d. Maximum principal tensile stress, σ_3, at the Earth's surface.*

It follows that the absolute tension during the 2009 episode is unlikely to have reached greater depths than about 370 m. Given the uncertainty in the values used, we could set this upper limit for the absolute tension at a depth of about 400 m. The tension fractures may, of course, be much shallower than this; but they very unlikely to be deeper. These analytical results also mean that significant tensile stress must be at the surface; more specifically the tensile stress that the surface must be at least 2 MPa, if we assume that 2 MPa is the in-situ

tensile strength. The theoretical tensile stress, however, should normally be expected to exceed the in-situ tensile strength for fracture formation and must be maintained to some depth – at least some tens of metres and, preferably, hundreds of metres so as to generate the tension fractures. Thus, if the dyke-induced tensile stress at the surface is only 2-3 MPa and diminishes at a shallow depth, such a dyke is unlikely to have generated the tension fractures at the surface. And it is even less likely to have triggered slip on existing, or the formation of new, normal faults. While discussing the numerical results below, we assume that the tensile stresses at the surface, for fracture initiation at the surface, must have, theoretically, reached several mega-pascals. As we shall also see in the numerical models below, there are further constraints on the mechanics of fracture formation, if triggered by dyke emplacement, in that while normal faulting and tension fractures occurred at the western boundary of the 'graben', only tension fractures were generated at the eastern boundary during the 2009 episode.

7. Numerical models

We used the finite-element software Comsol Multiphasic (www.comsol.com) for a general analysis of the local stresses associated with arrested dykes, with application to the inferred arrested 2009 dyke. All the models are fastened in the corners, as indicated by crosses (Fig. 13a), so as to avoid rigid-body rotation and translation. In all the models the only loading is internal magmatic overpressure (driving pressure) of 6 MPa (cf. Eq. 2). This value is within the range of a typical in-situ tensile strength of rocks (Gudmundsson, 2011a). We do not use a higher overpressure because we assume the dyke to be basaltic, so that, in a continental crust like here, the buoyancy term may not add much overpressure to excess pressure at the time of magma-chamber or reservoir rupture (Eq. 2). In all the models, the lower tip (bottom) of the dyke is at the depth of about 10 km, whereas the upper tip or top is at depths of 0.3, 0.5, and 1 km below the surface. As indicated above the dip dimension may be 15-20 km but for the purpose of modelling effects of shallow layering on surface stresses, the dip dimension used here is appropriate.

In the first models, the crust has the same uniform properties. This is shown by all the indicated layers having the same Young's modulus (here 40 GPa). This means that the first models are elastic half-space models, as are still the most commonly used to model surface stresses and deformation associated with volcanic unrest periods (e.g., Dzurisin, 2006; Segall, 2010). For the models presented in this paper, all the layers and units have the same Poisson's ratio, namely 0.25, which is the most common ratio for rocks (Gudmundsson, 2011a). Variations in Poisson's ratio of rocks are generally very small (normally by a factor of 2 or less) so as to be negligible in comparison with the variation in Young's modulus or stiffness; the latter may easily vary by 2 orders of a magnitude in any volcanic zone/volcanic edifice, and sometimes by 3 orders of a magnitude. In later models, we have realistic layering with Young´s modulus in different layers ranging from 1 GPa, for soft layers, to 40 GPa for stiff layers. This range is presumably smaller than the actual range in crustal segments such as that hosting Harrat Lunayyir, but serves the purpose of illustrating the effects of reasonable layering on surface stresses and likely fracture formation induced by arrested dykes such as the one in 2009.

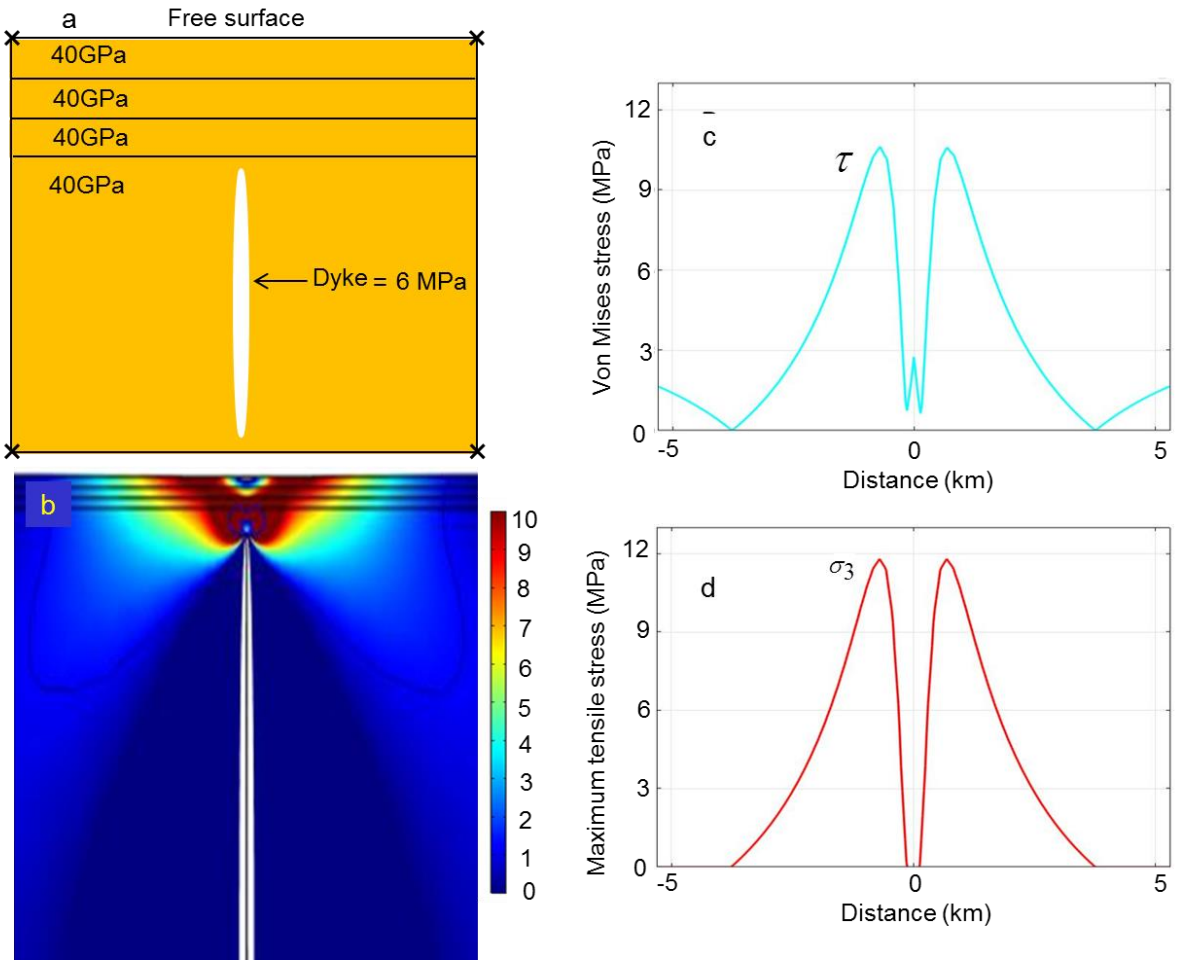

Fig. 14. *Numerical model of a dyke arrested with a tip at the depth of 500 m below the Earth's surface. The magmatic overpressure is 6 MPa and Poisson's ratio of all the rock layers is 0.25. Each of the 3 top layers is 100 m thick. All the 3 top layers, as well as the main rock unit hosting the dyke have the same Young's modulus of 40 GPa. Thus, this is effectively an elastic half-space model. a. Schematic setup of the model. The thickness of the layers and the height of the dyke are not to scale. b. Maximum principal tensile stress, σ_3, in mega-pascals (range shown 0-10 MPa). c. 16 d. Maximum principal tensile stress, σ_3, at the Earth's surface.*

In the layered models, each of the layers that constitute the uppermost part of the crust is 100 m thick. This thickness remains constant in all the models. Also, in all the models the lowermost layer or unit hosts most or all of the dyke. (Depending on how shallow the dyke tip is, the top part of the dyke penetrates some of the shallow layers in some of the models.) Young's modulus of these shallow layers derives from seismic data, where we calculate the dynamic Young's modulus based on the velocities of the seismic waves (Jaeger and Cook, 1979). The dynamic moduli are 27 GPa for two of the layers and 17 GPa for the surface layer. The layer or unit hosting (most of) the dyke has a dynamic Young's modulus of 40 GPa. These values are primarily based on seismic velocities in Harrat Lunayyir, but are within the range of laboratory determined Young's moduli for granites and other typical

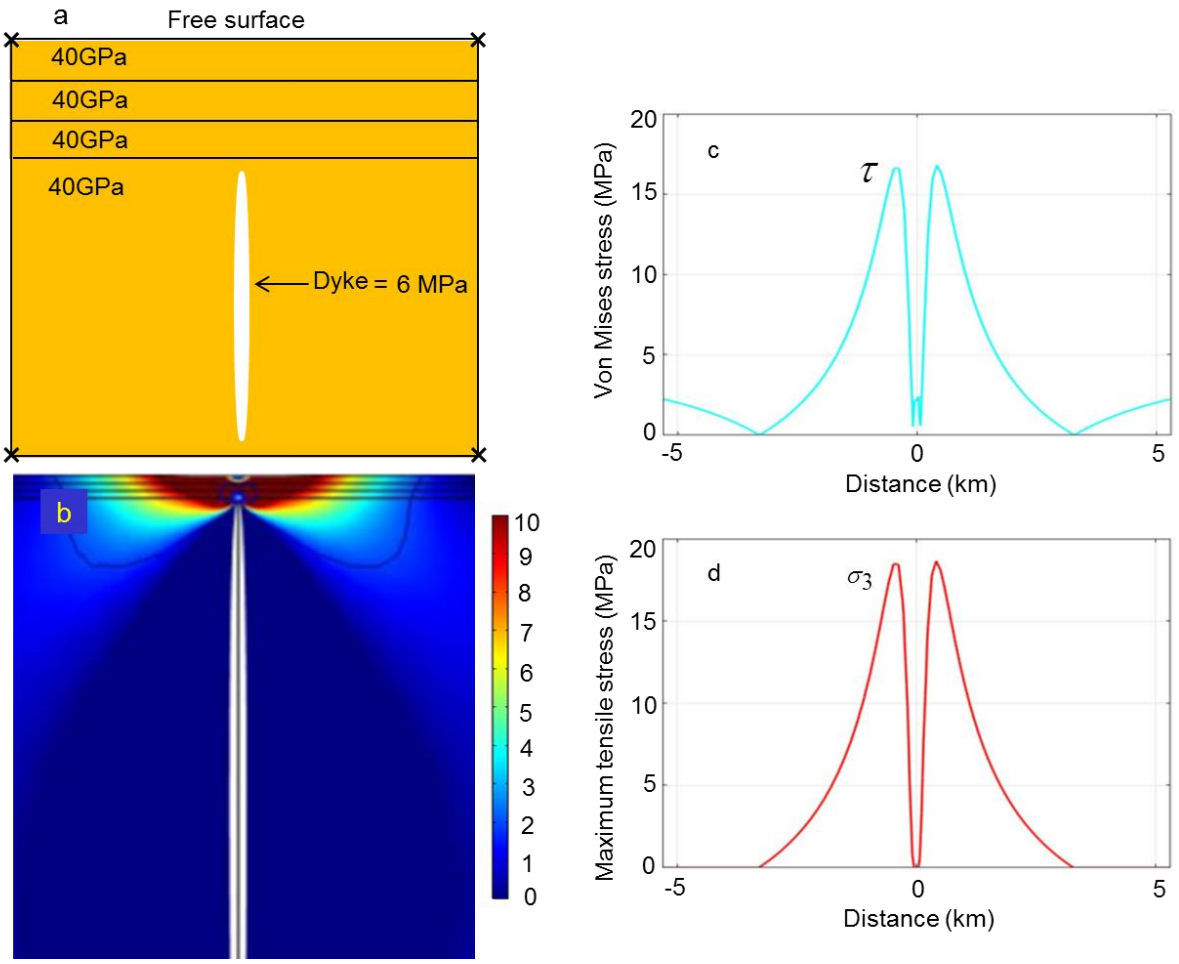

Fig. 15*. Numerical model of a dyke arrested with a tip at the depth of 300 m below the Earth's surface. The magmatic overpressure is 6 MPa and Poisson's ratio of all the rock layers is 0.25. Each of the 3 top layers is 100 m thick. All the 3 top layers, as well as the main rock unit hosting the dyke have the same Young's modulus of 40 GPa. Thus, this is effectively an elastic half-space model. a. Schematic setup of the model. The thickness of the layers and the height of the dyke are not to scale. b. Maximum principal tensile stress, σ_3, in mega-pascals (range shown 0-10 MPa). c. von Mises shear stress at the Earth's surface. d. Maximum principal tensile stress, σ_3, at the Earth's surface.*

continental rocks (Gudmundsson, 2011a) and thus reflect more general conditions. In later layered models we use still more realistic layering, where comparatively soft layers, with Young's modulus of 1-3 GPa, form part of the crustal segment. The layer thickness of 100 m is somewhat arbitrary in that it would generally reflect 'seismic layers', that is, groups of layers with similar seismic/mechanical properties. Some sedimentary layers and some lava flows, such as pahoehoe, may reach 100 m thickness, but here this thickness should be interpreted as mechanical/seismic rather than lithological.

In all the models, we show the layering (and lack of layering in the first models) to illustrate the assumed general structure of the crust. The layers are shown in the a-part of each model figure, which also gives the Young's modulus of each layer. The location of the dyke tip, however, is not changed in the a-parts of the figures; the dyke is there always shown

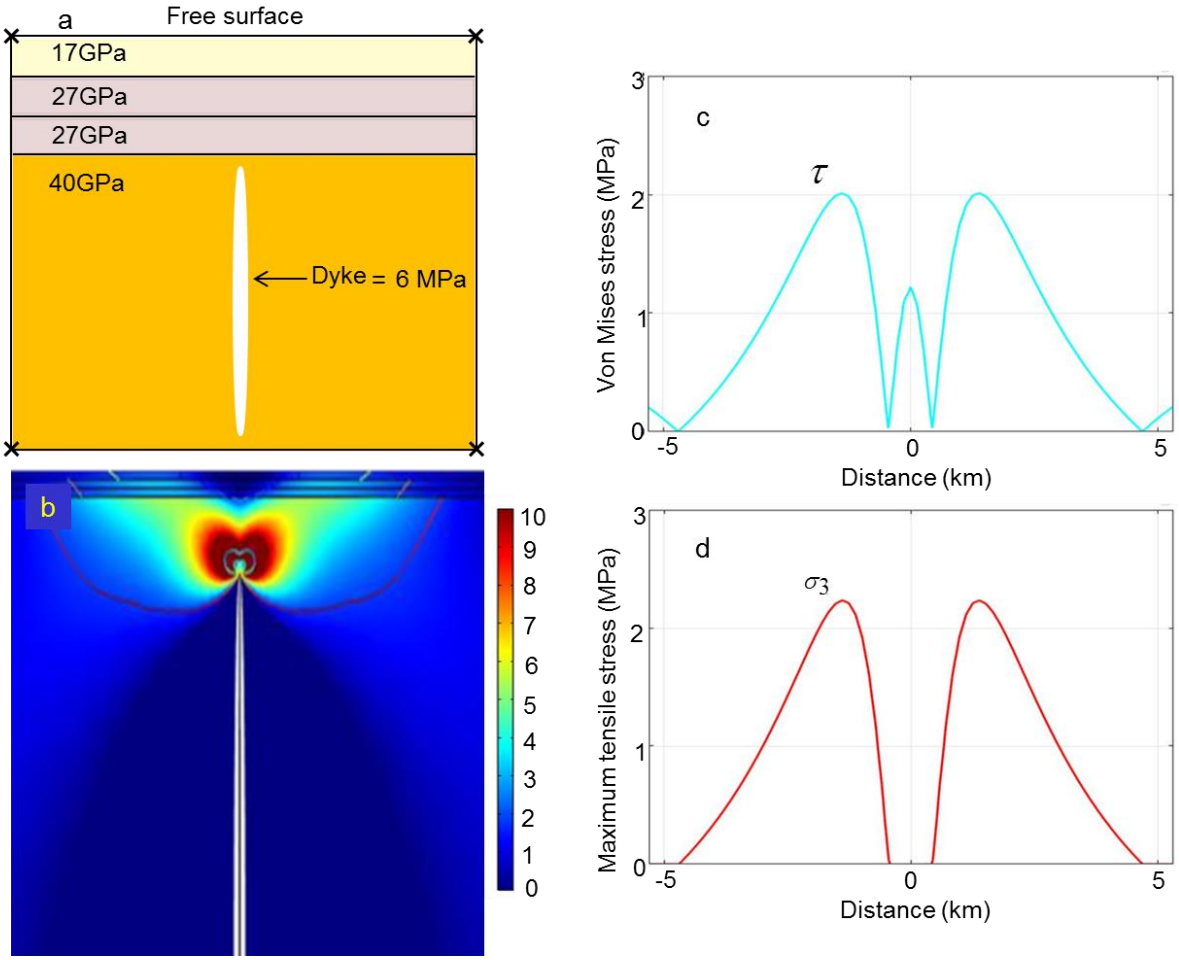

Fig. 16. *Numerical model of a dyke arrested with a tip at the depth of 1000 m below the Earth's surface. The magmatic overpressure is 6 MPa and Poisson's ratio of all the rock layers is 0.25. Each of the 3 top layers is 100 m thick. The surface layer has Young's modulus of 17 GPa, followed by two layers with a Young's modulus of 27 GPa. The unit or layer hosting the dyke has a Young's modulus of 40 GPa. a. Schematic setup of the model. The thickness of the layers and the height of the dyke are not to scale. b. Maximum principal tensile stress, σ_3, in mega-pascals (range shown 0-10 MPa). c. von Mises shear stress at the Earth's surface. d. Maximum principal tensile stress, σ_3, at the Earth's surface.*

at the same location because the main aim of the a-parts is to show the layering. The b-parts of the figures show the exact location of the dyke tip, which in some of the later models penetrates the lowermost of the 3-4 top layers.

The early models have 3 layers above the thick layer or unit hosting (most of) the dyke. In the later models, however, we have added one additional layer, which is white in all the models and with a Young's modulus or stiffness of 1 GPa. In-situ Young's modulus of 1 GPa is common among many compliant pyroclastic and sedimentary rocks (Gudmundsson, 2011a). For example, many soil, sediment, and scoria layers between lava flows have similar or lower Young's moduli. Here we assume the layer to be of the same thickness as the other layers, namely 100 m. In most crustal segments there are certainly layers much thinner than

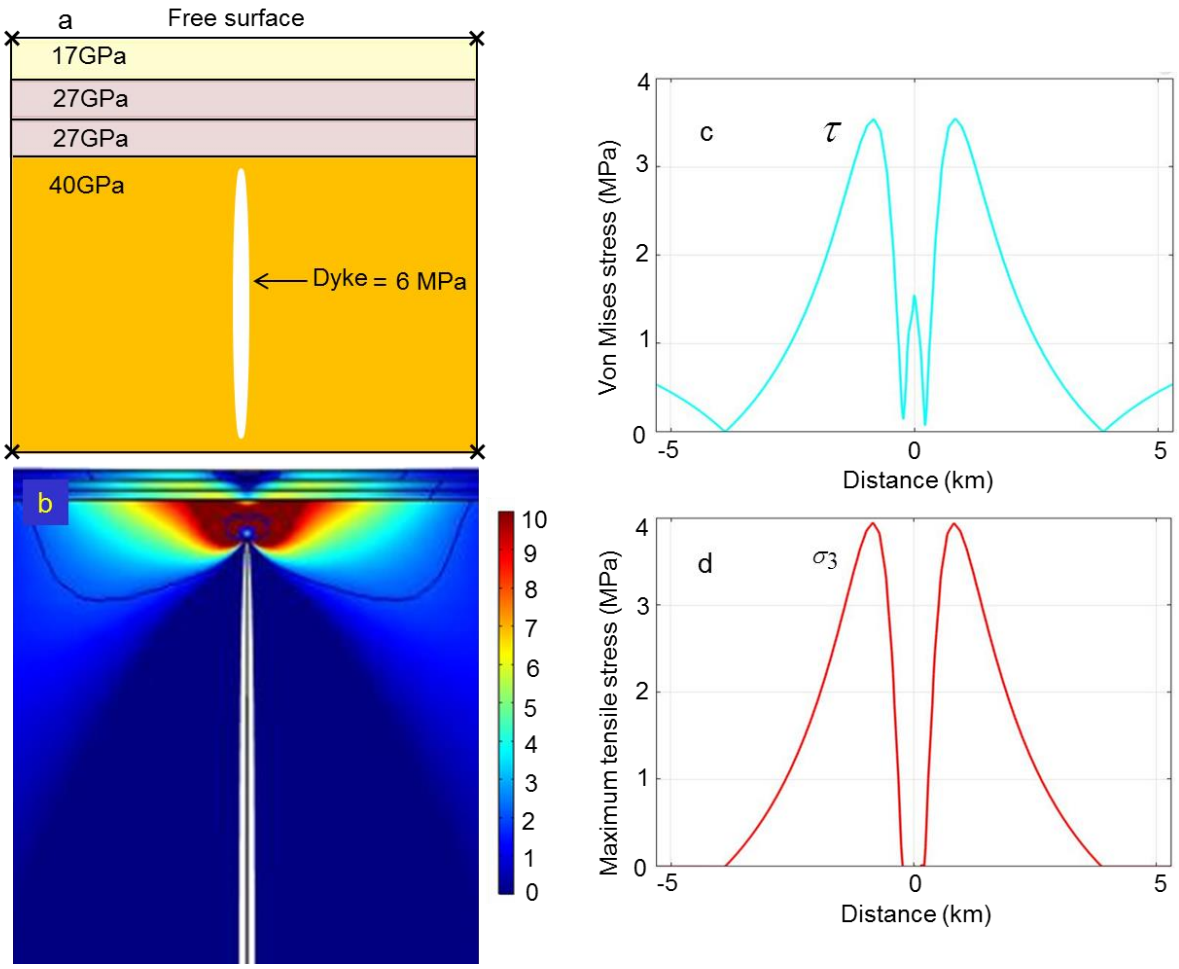

Fig. 17. *Numerical model of a dyke arrested with a tip at the depth of 500 m below the Earth's surface. The magmatic overpressure is 6 MPa and Poisson's ratio of all the rock layers is 0.25. Each of the 3 top layers is 100 m thick. The surface layer has Young's modulus of 17 GPa, followed by two layers with a Young's modulus of 27 GPa. The unit or layer hosting the dyke has a Young's modulus of 40 GPa. a. Schematic setup of the model. The thickness of the layers and the height of the dyke are not to scale. b. Maximum principal tensile stress, σ_3, in mega-pascals (range shown 0-10 MPa). c. von Mises shear stress at the Earth's surface. d. Maximum principal tensile stress, σ_3, at the Earth's surface.*

100 m – some as thin as metres or tens of centimetres – but for the purpose of illustrating the principles that control dyke-induced surface deformation the thickness used here is for the seismic/mechanical top layers is appropriate. In the absence of detailed knowledge of the actual layering of the crust of Harrat Lunayyir – to which these models are applied - these thicknesses are suitable (we add a soft layer in later models), in particular because the main mechanical effect of a layer does not lie in its thickness but rather in its softness or compliance. In the models, we vary the depth of the 1GPa layer so as to explore the effect its depth would have on the dyke-induced surface stresses and associated deformation.

In the first model (Fig. 13) the dyke tip is arrested at 1 km depth below the surface. Here all the layers have the same Young's modulus, 40 GPa, so that the modelled crust is

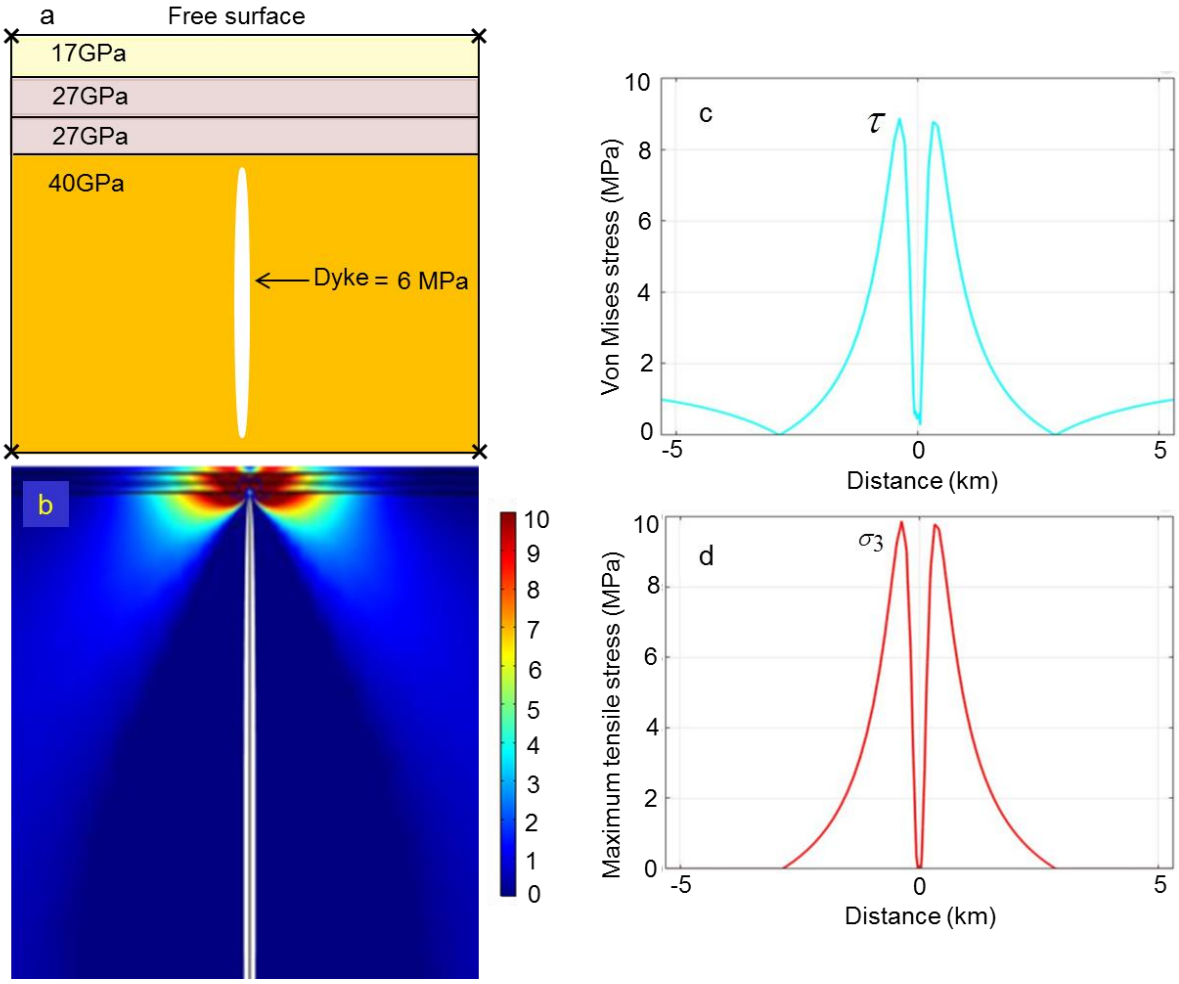

Fig. 18. *Numerical model of a dyke arrested with a tip at the depth of 300 m below the Earth's surface. The magmatic overpressure is 6 MPa and Poisson's ratio of all the rock layers is 0.25. Each of the 3 top layers is 100 m thick. The surface layer has Young's modulus of 17 GPa, followed by two layers with a Young's modulus of 27 GPa. The unit or layer hosting the dyke has a Young's modulus of 40 GPa. a. Schematic setup of the model. The thickness of the layers and the height of the dyke are not to scale. b. Maximum principal tensile stress, σ_3, in mega-pascals (range shown 0-10 MPa). c. von Mises shear stress at the Earth's surface. d. Maximum principal tensile stress, σ_3, at the Earth's surface*

analogous to a homogeneous and isotropic elastic half space, a type of model still very common in volcano-deformation studies. The results (Fig. 13c, d) show that the surface shear stress and tensile stress reach close to 6 MPa. Both stresses are large enough to have the potential of generating or initiating fractures at the surface. We think, however, that the dyke became arrested at much shallower depth, at about 500 m or perhaps as little as 300 m below the surface. This follows partly from the analytical considerations above, and is used as a basis in many of the numerical models below. We therefore made another elastic half-space model with the dyke tip at, first, the depth of 500 m (Fig. 14) and, then, at the depth of 300 m

(Fig. 15). The results (Fig. 14-15) show that the surface stresses reach up from 10-12 MPa, for 500 m tip depth, up to 17-18 MPa, for 300 m tip depth.

In these models the stiffnesses (Young's modulus) of some of the layers are unrealistically high. This applies, in particular, to the surface layer; 40 GPa is far too high for the surface layers in Harrat Lunayyir, where a dynamic modulus of 10-20 GPa would be more reasonable for some of the surface layers, with the static modulus much lower, as discussed below. But for an elastic half-space model such as this one, there must be a uniform Young's modulus, and 40 GPa is reasonable to the average stiffness of the part of the crustal segment dissected by the dyke. Thus, even if the surface stresses reach something like 17 MPa, the high stiffness of the surface layers (which tends to raise the stresses) is unrealistic, making the calculated stress values unrealistic as well.

In the next model (Fig. 16) the crust is layered in the simplest possible way. There are 3 layers that constitute the uppermost part (300 m) of the crust. Two have a Young's modulus of 27 GPa, and the surface layer a Young's modulus of 17 GPa. These values, also used in subsequent models, are based on the considerations of the dynamic mechanical layering in Harrat Lunayyir, discussed above. These are likely to be crude average dynamic values. The unit hosting the dyke is, as before, with a stiffness of 40GPa. The results (Fig. 16) show that for dyke arrested with a tip at 1 km depth and the simplest type of layering, the induced maximum theoretical tensile and shear stresses at the surface are only about 2 MPa, and thus generally too small to generate fractures, either tension fractures or normal faults.

Even when the dyke tip is arrested at the depth of 500 m, for the same layering, the surface stresses are so low as to be unlikely to generate surface fractures (Fig. 17). In fact, it is only when the dyke tip has reached the very shallow depth of 300 m that the surface stresses become high enough so as to have a chance of generating fractures (Fig. 18). Here the surface stresses reach 9-10 MPa. These stresses are certainly high enough to generate tension fractures. Whether initiated tension fractures might change into small normal faults would then depend on the depths to which they could propagate. In the model in Fig. 18 the tensile stresses are comparatively high to depths in excess of 300 m (the red zones in part b) so that, based on the conclusions in Section 6, some of the tension fractures might change into normal faults.

The models above, Figs. 16-18, while mechanically perfectly valid, are geologically perhaps not as realistic as such models can be made. In all crustal segments there are compliant or soft layers (with low Young's modulus) in-between stiffer layers. This applies particularly to volcanically active areas where soft pyroclastic, sediment, and soil layers are common in-between stiffer units such as lava flows. Such layers are known to have very great effects on the local stresses induced by dykes (Gudmundsson, 2002, 2003). The detailed crustal layering in Harrat Lunayyir is unknown, but must certainly include soft layers. In addition, the surface layer in the western part of the graben, where we studied the fractures in the field (Figs. 3-7), is partly compliant pyroclastics, with a Young's modulus of the order of a few giga-pascal (rather than 17 or 40 GPa used in the models above). On the eastern side of the graben, however, some of the tension fractures occur in comparatively stiff granitic rocks (Jonsson, 2012).

In order to take soft layers into account, and explore their effects on the dyke-induced stresses, we made several models with a single soft layer, 100 m thick and with a stiffness of

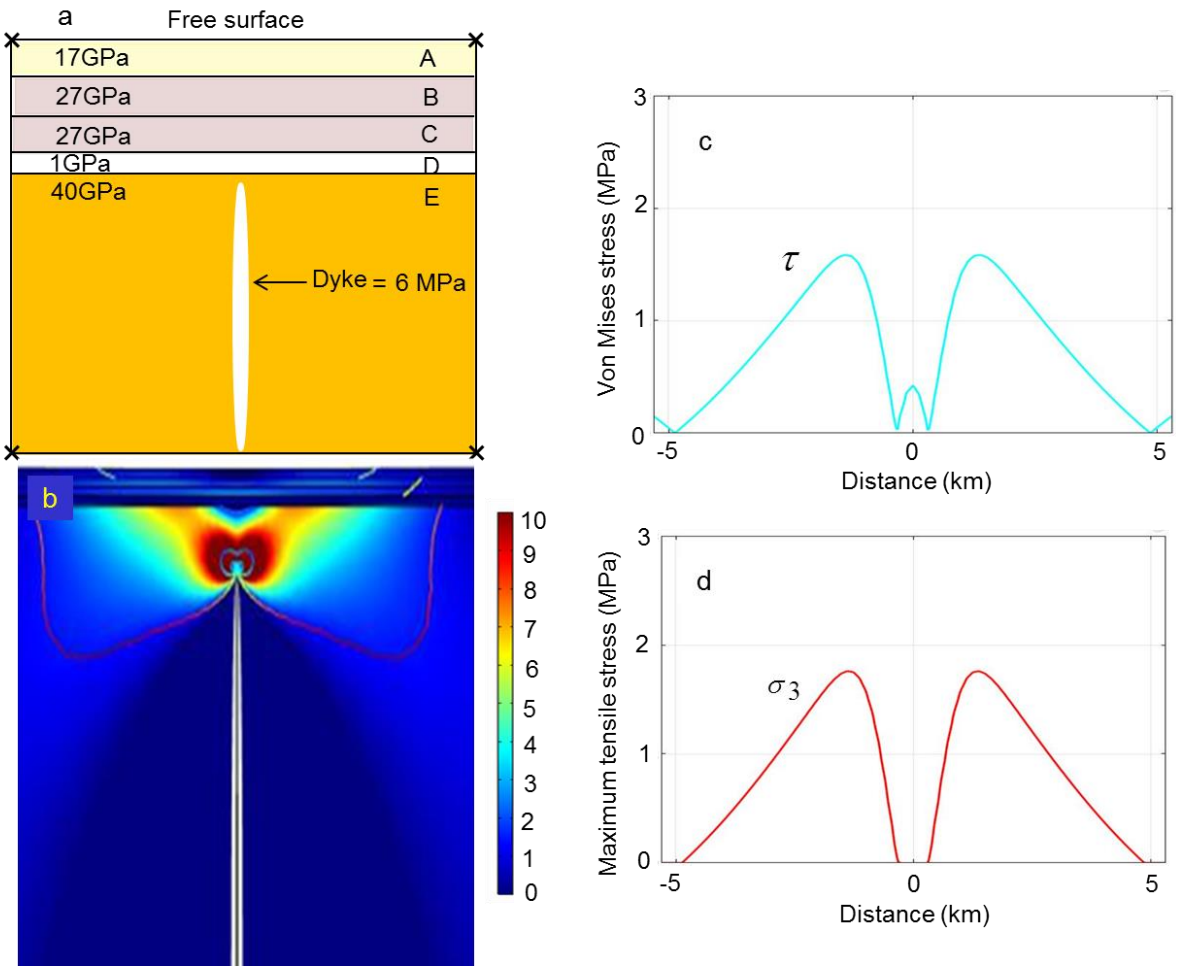

Fig. 19. *Numerical model of a dyke arrested with a tip at the depth of 1000 m below the Earth's surface. The magmatic overpressure is 6 MPa and Poisson's ratio of all the rock layers is 0.25. Each of the 4 top layers is 100 m thick. The surface layer has Young's modulus of 17 GPa, followed by two layers with a Young's modulus of 27 GPa. The unit or layer hosting the dyke has a Young's modulus of 40 GPa, and a fourth layer with a Young's modulus of 1 GPa. a. Schematic setup of the model. The thickness of the layers and the height of the dyke are not to scale. b. Maximum principal tensile stress, σ_3, in mega-pascals (range shown 0-10 MPa). c. von Mises shear stress at the Earth's surface. d. Maximum principal tensile stress, σ_3, at the Earth's surface.*

1 GPa. Such stiffness would be typical of many soft or compliant pyroclastic and sedimentary layers – many of which could, in fact, be much softer (Gudmundsson, 2011a). In the models we, as before, vary the depth of the dyke tip below the surface – the three depths considered are 1000 m, 500 m, and 300 m. But, in addition, we vary the location, that is, the depth of the soft layer itself from being with the top at the depth of 100 m, to being with the top a depth of 300 m. The results show that varying the depth of the soft layer has comparatively little effect on the surface stresses, which are, the stresses of greatest interest here. We therefore show only the results where the soft layer is at the maximum depth, 300 m, except for the last model of this kind, where the surface of the soft layer is at 100 m depth.

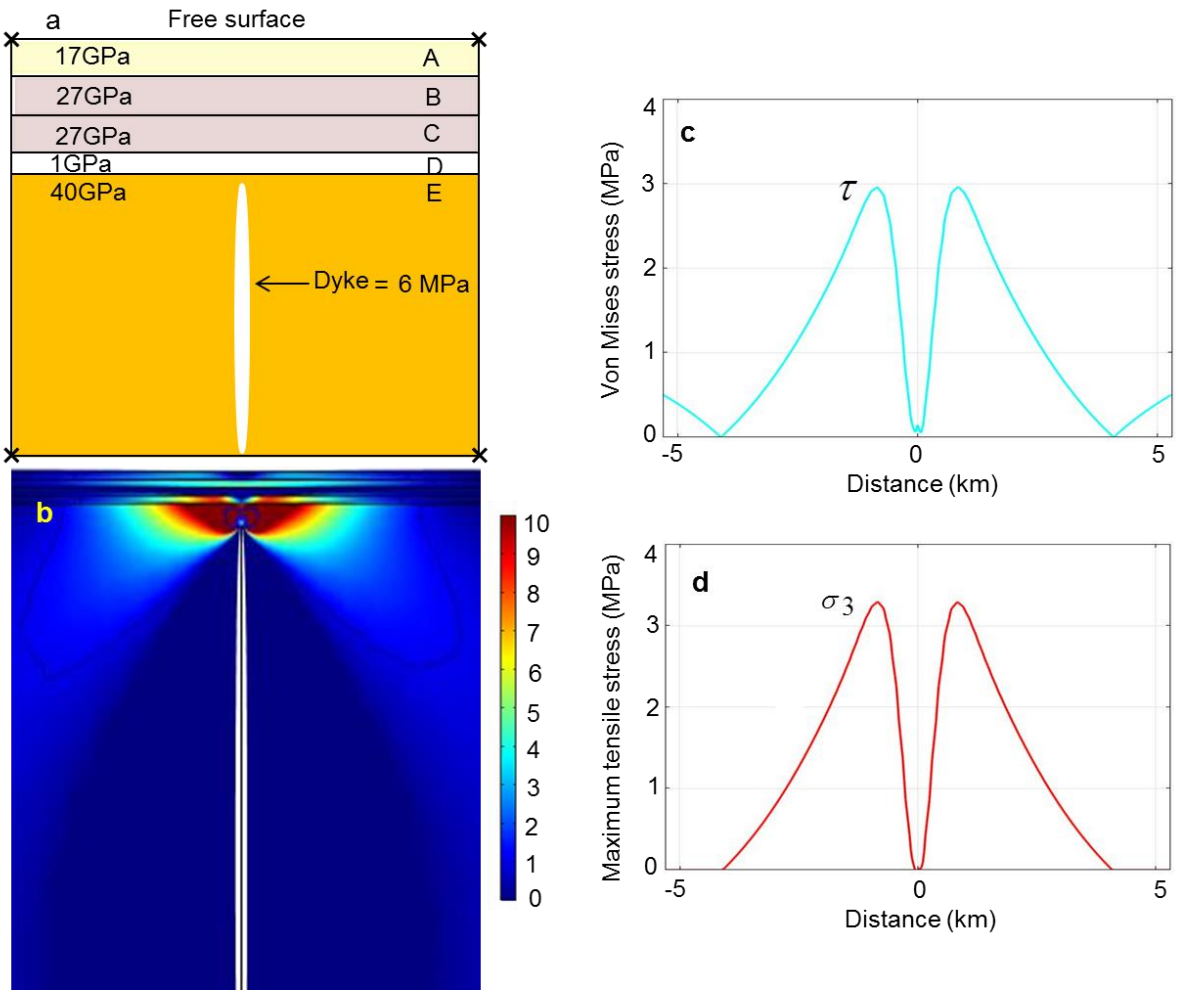

Fig. 20. *Numerical model of a dyke arrested with a tip at the depth of 500 m below the Earth's surface. The magmatic overpressure is 6 MPa and Poisson's ratio of all the rock layers is 0.25. Each of the 4 top layers is 100 m thick. The surface layer has Young's modulus of 17 GPa, followed by two layers with a Young's modulus of 27 GPa, and a fourth and compliant layer with a Young's modulus of 1 GPa. The unit or layer hosting the dyke has a Young's modulus of 40 GPa. a. Schematic setup of the model. The thickness of the layers and the height of the dyke are not to scale. b. Maximum principal tensile stress, σ_3, in mega-pascals (range shown 0-10 MPa). c. von Mises shear stress at the Earth's surface. d. Maximum principal tensile stress, σ_3, at the Earth's surface.*

The first model (Fig. 19) shows the stresses induced by a dyke whose tip is arrested at 1 km below the surface. The model shows very clearly the great effects of the soft layer on the crustal stresses. In particular, the soft layer basically suppresses all stresses, so that very low stresses are transmitted across the layer. The surface stresses (Fig. 19c,d) are well below 2 MPa, even if the surface layer at 17 GPa is still stiff. It follows from the low surface stresses that neither tension-fracture formation nor normal faulting is likely. The next model is identical except for the depth to the dyke tip, which is here at 500 m (Fig. 20). Even if the dyke tip is here very close to the surface, the surface stresses are still very low, the maximum

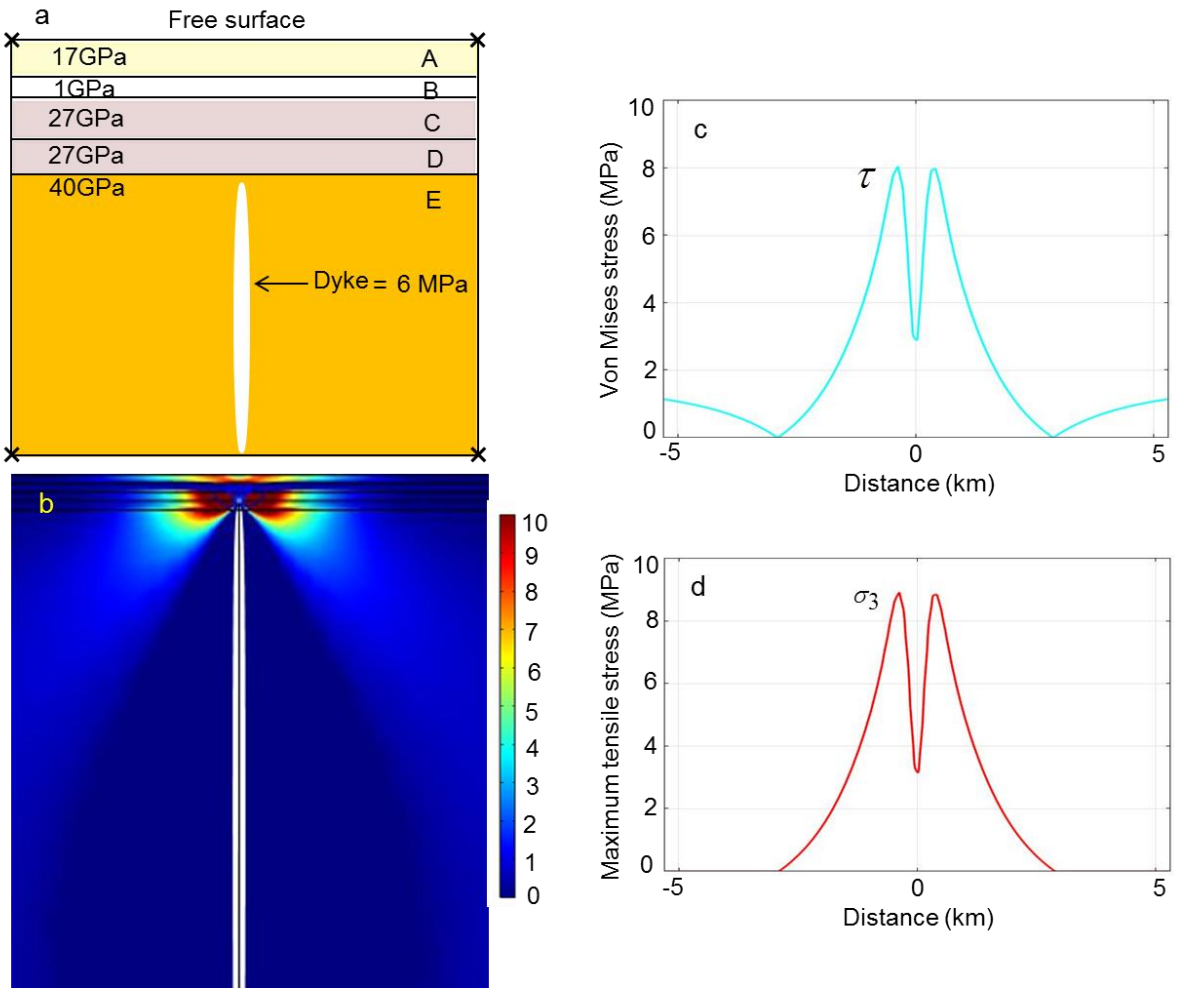

Fig. 21. *Numerical model of a dyke arrested with a tip at the depth of 300 m below the Earth's surface. The magmatic overpressure is 6 MPa and Poisson's ratio of all the rock layers is 0.25. Each of the 4 top layers is 100 m thick. The surface layer has Young's modulus of 17 GPa, followed by a compliant layer with a Young's modulus of 1 GPa, and then two layers with a Young's modulus of 27 GPa. The unit or layer hosting the dyke has a Young's modulus of 40 GPa. a. Schematic setup of the model. The thickness of the layers and the height of the dyke are not to scale. b. Maximum principal tensile stress,* σ_3*, in mega-pascals (range shown 0-10 MPa). c. von Mises shear stress at the Earth's surface. d. Maximum principal tensile stress,* σ_3*, at the Earth's surface.*

being around 3 MPa. Thus, even at such a shallow dyke-tip depth, much dyke-induced surface fracturing is unlikely.

We did not make a model with the dyke tip at 300 m depth for this layering, because then the tip of the dyke would have entirely penetrated the soft layer, thereby making its effect on the stress field minimal. Instead, we show here the dyke tip at 300 m depth, but the soft 1 GPa layer is with a top at 100 m depth below the surface, that is, the soft layer is the second layer from the surface (Fig. 21). The stress-suppressing effects of the soft layer are still very noticeable. Nevertheless, because the dyke tip is so close to the surface, the maximum dyke-

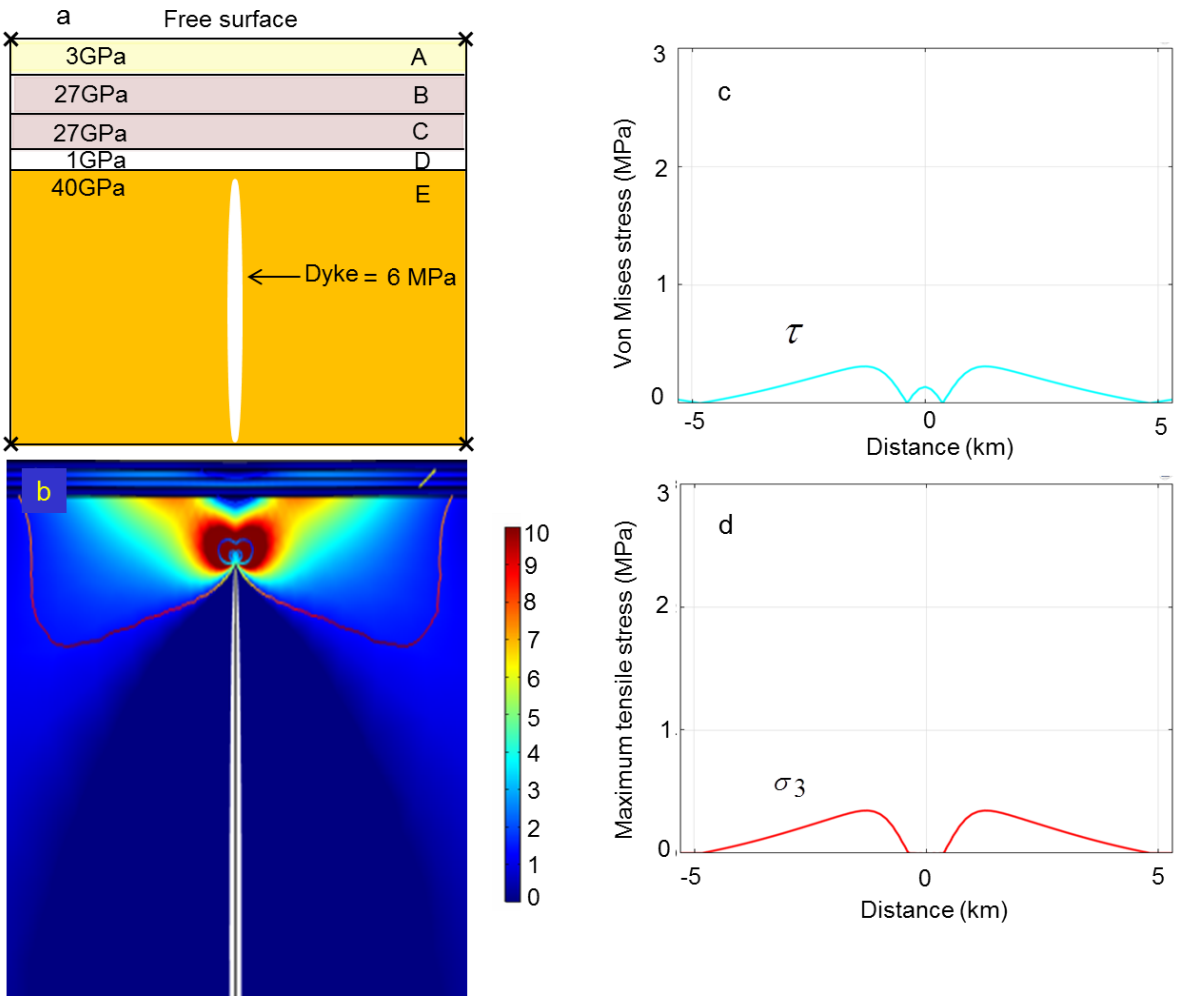

Fig. 22. *Numerical model of a dyke arrested with a tip at the depth of 1000 m below the Earth's surface. The magmatic overpressure is 6 MPa and Poisson's ratio of all the rock layers is 0.25. Each of the 4 top layers is 100 m thick. The surface layer has Young's modulus of 3 GPa, followed by two layers each with a Young's modulus of 27 GPa, and then a compliant layer with a Young's modulus of 1 GPa. The unit or layer hosting the dyke has a Young's modulus of 40 GPa. a. Schematic setup of the model. The thickness of the layers and the height of the dyke are not to scale. b. Maximum principal tensile stress, σ_3, in mega-pascals (range shown 0-10 MPa). c. von Mises shear stress at the Earth's surface. d. Maximum principal tensile stress, σ_3, at the Earth's surface.*

induced surface stresses reach just over 8 MPa. These stresses would normally be able to initiate tension fractures and normal faults.

In all the models presented above, the surface layer has stiffness or Young's modulus of 17 GPa. This value, like that of other moduli here, is primarily based on seismic velocity considerations, that is, it is a dynamic modulus. While dynamic moduli are very suitable for the propagation of an earthquake rupture – whose rate is similar to that of an the S-wave, that is, several kilometres per second – for dyke propagation static moduli are normally much more appropriate. This follows because dyke propagation rates are of the order of metres per second or less and thus many orders of magnitude slower than the velocities of seismic

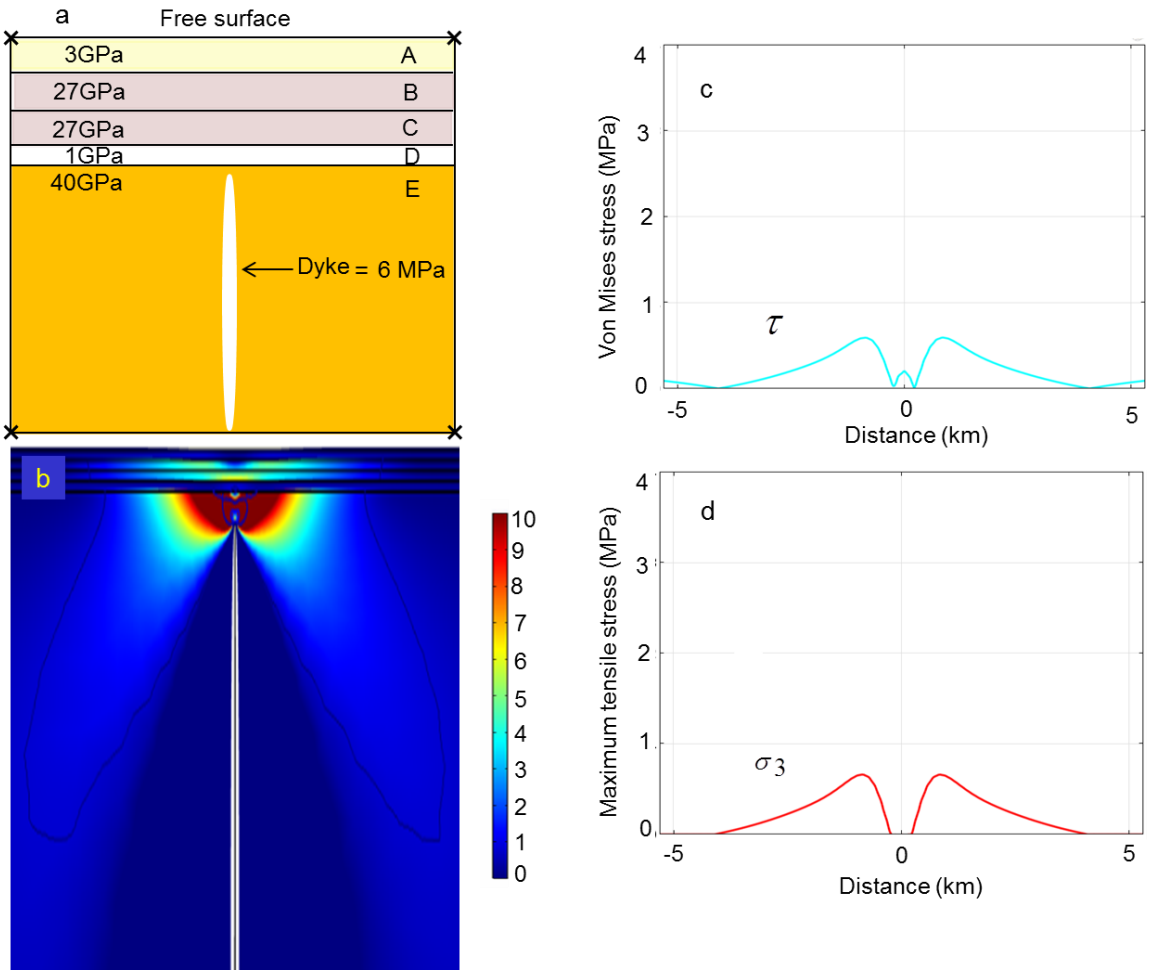

Fig. 23. *Numerical model of a dyke arrested with a tip at the depth of 500 m below the Earth's surface. The magmatic overpressure is 6 MPa and Poisson's ratio of all the rock layers is 0.25. Each of the 4 top layers is 100 m thick. The surface layer has Young's modulus of 3 GPa, followed by two layers each with a Young's modulus of 27 GPa, and then a compliant layer with a Young's modulus of 1 GPa. The unit or layer hosting the dyke has a Young's modulus of 40 GPa. a. Schematic setup of the model. The thickness of the layers and the height of the dyke are not to scale. b. Maximum principal tensile stress, σ_3, in mega-pascals (range shown 0-10 MPa). c. von Mises shear stress at the Earth's surface. d. Maximum principal tensile stress, σ_3, at the Earth's surface.*

ruptures for which dynamic moduli are appropriate. The difference between static and dynamic Young's modulus varies from zero to a factor of about 13, and is normally highest at shallow depth in active areas (Gudmundsson, 2011a). This follows because at shallow depth in active areas the fractures (e.g. cooling joints) and cavities (pores, vesicles), and contacts are normally not yet filled with secondary minerals, and discontinuities and cavities of all kind lower the static modulus but have much less effect on the dynamic modulus.

Considering also the soft surface layers seen on many of the photographs (Figs. 3-8), we decided to run several models with a comparatively soft or compliant surface layer. In these models, the surface layer has a Young's modulus of 3 GPa. This is similar to that of many

comparatively compliant layers, such as young lava flows, pyroclastic layers, and sedimentary layers (Gudmundsson, 2011a). We also include the earlier soft layer, 1GPa. For the first two models, the 1GPa layer is the fourth from the top, that is, with a top surface at the depth of 300 m, so as to be in agreement with the models above (Figs. 19 and 20). In the last model, however, where the dyke tip is at the depth of 300 m, the 1GPa layer is with its top surface at 100 m depth, as in the model in Fig. 21.

The results of the first model with this layering has a dyke tip at 1000 m depth and shows that very little stress reaches the surface (Fig. 22). The maximum tensile and shear stresses at the surface are only about 0.4 MPa, and would normally not result in any fracture formation. Very similar results are obtained for a dyke tip at 500 m depth. The surface stresses are about 0.7 MPa and thus generally too low to generate either tension fractures or normal faults. In the last model, the dyke tip is at a depth of 300 m so that the 1GPa layer is with a top at 100 m depth. Even if the dyke tip is only 300 m below the surface, the surface stresses are low – just about 2 MPa (Fig. 24). Some minor surface fracturing is possible, but major tension fractures and normal faults are unlikely to be generated in this stress field.

8. Dimensions of the 2009 dyke

The dimensions of the dyke inferred to have been emplaced during the 2009 episode can be estimated using various methods. The main methods that have been used are the distribution of associated earthquakes and geodetic data. Several estimates have been made. Baer and Hamiel (2010) give the dyke strike dimension or length as 12 km, the maximum dyke thickness as 2.5 m, and the dyke dip dimension or depth as about 10 km. However, they also use dyke segments with cumulative dip dimension of 15 km. The projection line of the hypocentres of the earthquakes, primarily associated with the dyke emplacement, during the 2009 episode is about 17 km long (Baer and Hamiel, 2010, fig. 1b).

Jonsson (2012) and Xu et al. (2016) infer that the tension fractures and faults at the surface were in zones as long as 14 km; in particular, Jonsson (2012) states that a normal fault on the western side of the ‘graben’ reaches this length. Presumably these authors interpret that strike dimension or length of the dyke as similar to this, or about 14 km. Xu et al. (2016) conclude that the depth to the dyke source was at least 20 km, and perhaps 35 km, so that the dyke dip dimension, while the dyke was continuously open, must, in their model, have been in this range. Their maximum dyke thickness is 2.3 m.

Our interpretation is that the dip dimension of the dyke is at least 20 km. The fact that the dyke continued to expand after it became arrested shows that the entire dip dimension was open at that time, and thus functioning as continuous fracture. For our modelling purposes it is enough to know that the dyke dip dimension is at least 20 km; this means that its dip dimension is larger than the strike dimension (given in a moment), so that the strike dimension is the ‘controlling dimension’, that is, the dimension that controls the thickness or opening of the dyke (Gudmundsson, 2011a). The strike dimension, based on the earthquake distribution (e.g. Baer and Hamiel, 2010), is most likely between 13 and 14 km (Fig. 8b). We take it as 14 km and conclude that the strike dimension is the controlling dimension.

To estimate the maximum opening or thickness of the dyke, in any layer or unit with a given Young’s modulus and Poisson’s ratio, we can either use the part-through crack model

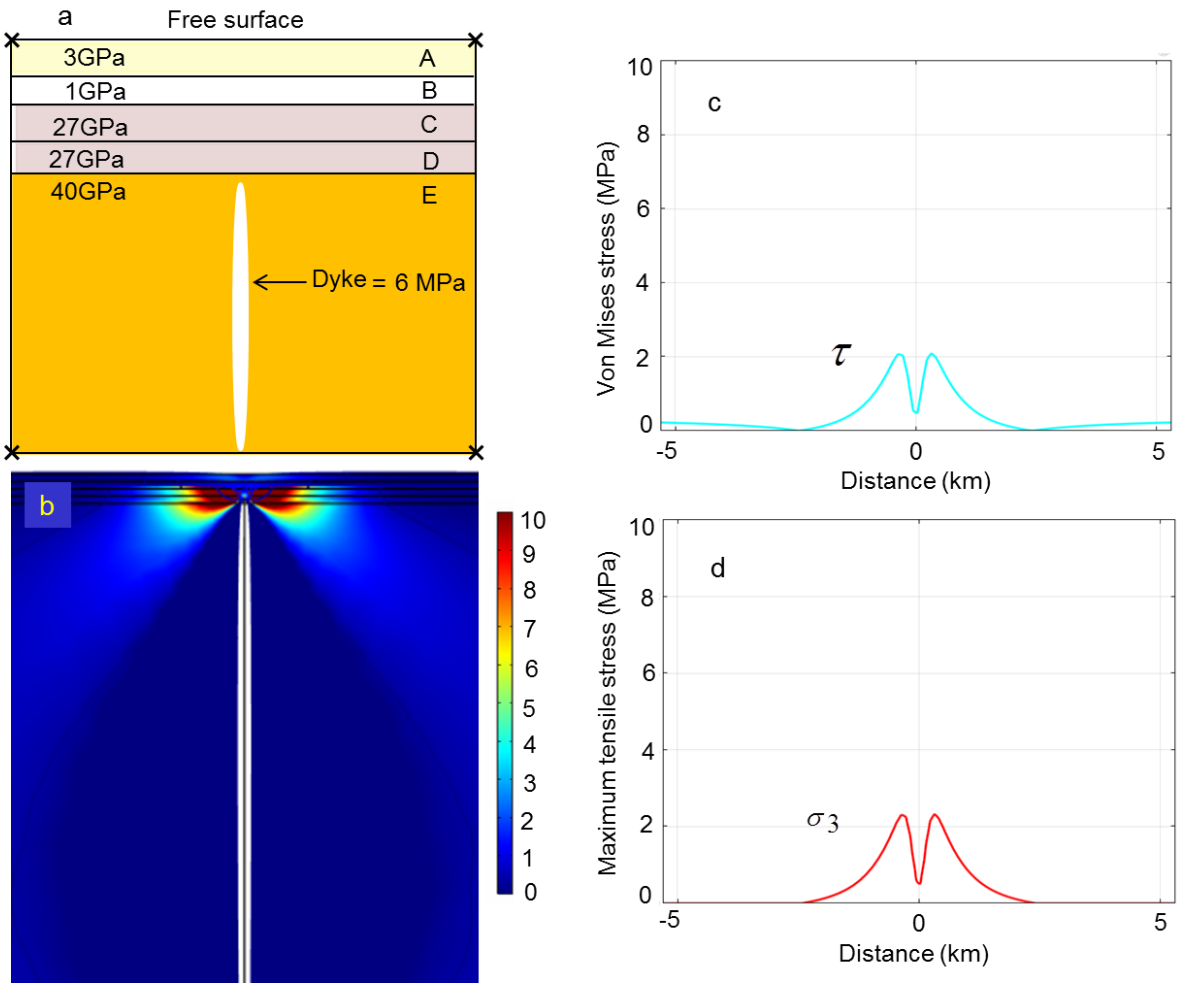

Fig. 24. *Numerical model of a dyke arrested with a tip at the depth of 300 m below the Earth's surface. The magmatic overpressure is 6 MPa and Poisson's ratio of all the rock layers is 0.25. Each of the 4 top layers is 100 m thick. The surface layer has Young's modulus of 3 GPa, followed a compliant layer with a Young's modulus of 1 GPa, and then by two layers each with a Young's modulus of 27 GPa. The unit or layer hosting the dyke has a Young's modulus of 40 GPa. a. Schematic setup of the model. The thickness of the layers and the height of the dyke are not to scale. b. Maximum principal tensile stress, σ_3, in mega-pascals (range shown 0-10 MPa). c. von Mises shear stress at the Earth's surface. d. Maximum principal tensile stress, σ_3, at the Earth's surface.*

or the through-crack model. The part-through model is commonly used for non-feeder dykes (Gudmundsson, 2011a). However, in the present case the dyke presumably became arrested at a mechanically weak contact, perhaps partly an open contact – given that the contact of arrest may have been as shallow as 300 m below the surface. In such a case, the through-crack model is a good approximation, and we used it here. The maximum opening of the dyke, or thickness, Δu_I is then given by (Gudmundsson, 2011a):

$$\Delta u_I = \frac{2 p_o (1-\nu^2) L}{E} \qquad (8)$$

where p_o is the magmatic overpressure or driving pressure, v is Poisson's ratio and E is Young's modulus of the layer/unit where the dyke thickness is to be determined, and L is the strike dimension or length of the dyke where the thickness/opening is determined.

Using the same values as in our numerical models, the main unit hosting the dyke has a Young's modulus of 40 GPa and a Poisson's ratio of 0.25. For a magmatic overpressure of 6 MPa and a dyke length or strike dimension of 14 km, the maximum thickness, from Eq. (8), would be about 3.9 m. At shallower depths, where the main layers have a Young's modulus of 27 GPa, the maximum opening or thickness of a dyke with the same length and overpressure would be about 5.8 m. And the dyke would be even thicker where hosted by very soft layers, such as 1GPa in the model in Fig. 23. However, we believe that the dyke would tend to become arrested on meeting the very soft layers, so here we assume that the main uppermost part of the dyke would be in the layers with a stiffness of 27 GPa. As indicated above, these are dynamic stiffnesses, so that the static stiffness could easily be half this value or less (Gudmundsson, 2011a), yielding a dyke thickness of 11.6 m.

A maximum thickness of 5.8-11.6 m for a 14 km long dyke would yield a length/thickness ratio between about 2400 and 1200. This is similar to the measured length/thickness ratios of regional basaltic dykes in Iceland, which range from about 300 to about 2000 (Gudmundsson, 1986). The dykes in Iceland are exposed at depths of 500-1500 m below the original surface of the volcanic zones within which they were emplaced so, again, rather similar to the uppermost part of the 2009 dyke. The length/thickness ratios of dykes depend primarily on host-rock Young's modulus and magmatic overpressure, but measured dykes worldwide have commonly ratios similar to those reported for the Icelandic dykes (Rickwood, 1990).

Thus, in our interpretation, the 2009 dyke is much thicker than previous models would indicate. Elastic half-space models, such as dislocation models of dykes, tend to underestimate dyke thicknesses. This follows because, by definition, these models assume no layering or contacts in the crust, thereby ignoring any stress 'dissipation' and suppression that the layering normally gives rise to (Figs. 13-24). Consequently, the half-space dislocation models overestimate the surface stresses and displacements supposed to be generated by a dyke of a given thickness. Our interpretation of the dyke thickness in relation to its other dimensions is very plausible based on worldwide studies of length/thickness ratios of dykes, as indicated above.

9. Discussion

9.1 General implications

While the numerical models are here applied to the 2009 volcanotectonic episode at Harrat Lunayyir in Saudi Arabia, the results are completely general. Here we first discuss some of the general implications, and then those that apply particularly to the episode at Harrat Lunayyir. Some of the main results for dyke-induced stresses and surface deformation in an active volcanic zone may be summarised as follows:

- Unless there is great mechanical heterogeneity in the crustal segment within which the dyke is emplaced, the stresses and the related deformation should be symmetric. A highly asymmetric surface deformation, even in layered and anisotropic crust, is thus unlikely to be induced by a single dyke.
- The distance between the two surface-stress peaks, where dyke-induced fractures would be possible in case the maximum stresses reaches at least several mega-pascals, is similar to twice the depth to the top of the dyke below the surface. This is a well-known result from earlier studies, sometimes referred to as the 'graben rule' and confirmed by analytical and numerical studies (Figs. 13-24). The only exception to this rule is if the Gook-Gordon delamination occur – a mechanism mostly limited to very shallow depths - so that the contact between layers opens up. Then the stresses at the surface normally peak above the lateral ends of the opened-up contact and would not have any correlation with the depth to the top of the dyke (Gudmundsson, 2003). In the present models, however, the contact is not weak enough to open up.
- It follows from the last point that, unless Cook-Gordon delamination operates, the half-width of a dyke-induced graben at the surface is similar to the depth to the top of the dyke. Thus, if a dyke-induced graben is 3 km wide, then the tip of the associated dyke would have to be at depth of close to 1.5 km. A dyke arrested at 1.5 km depth in an active volcanic zone would rarely induce large enough stresses at the surface to initiate fractures, major normal faults in particular. As we have seen in the models presented here, a crustal segment with one or several soft layers would commonly suppress any dyke-induced surface stresses to such an extent that only dykes arrested at very shallow depth – a few hundred metres or less – could possible trigger fracture formation at the surface.

9.2 Implications for the 2009 episode

The analytical and numerical models presented here do not support the suggestions that the entire surface-fracture formation and development during the 2009 episode was induced by an arrested dyke. The main reasons for this conclusion may be summarised as follows:

1. The graben in Fig. 8 is between 3 and 7 km wide. If we take an average width as 5 km, then that would imply that the dyke tip at the time of fracture formation was at a depth of more than 2 km (which is also the depth suggested by some of the authors of the cited papers). However, the numerical models presented here show that, for any reasonably layering, the surface stresses even at the depth of 1 km, let alone a depth of more than 2 km, would be too small to generate significant fractures. It is only when the tip reaches the shallow depth of 500 m, and, in particular, 300 m, that the surface stresses become large enough so as to generate significant fractures.
2. When the tip of the arrested dyke is at 300-500 m depth, clearly the graben that the dyke could initiate at the surface could not be wider than about 0.6-1 km. A graben of average width 5 km is simply too wide to be generated by the stresses induced by a dyke arrested at the depth of 300-500 m.

3. None of the main fractures coincide in strike with the inferred strike of the dyke and many strike very differently from that of the dyke (Fig. 8b).. Furthermore, some of the fractures apparently dissect the dyke, when its strike is projected (as a broken line) to the surface.
4. Although we have followed the established tradition in the literature on this episode and referred to the structure as a graben, the general fracture pattern supposed to have been generated in the 2009 episode does not follow the geometry of a classical graben. In fact, the 'boundary fault' on the eastern side of the 'graben' is not a fault but rather a zone of tension fractures. The symmetry of the stress field induced by an arrested dyke would tend to generate a clear graben structures, with two normal boundary faults, but that is not what happened here.

While there have, apparently, been no previous numerical models applied to the 2009 episode (dislocation models of the dyke applied by many authors are, strictly, analytical models), some authors have used analogue models to explain the surface fracture pattern. Analogue models in structural geology and volcanotectonics, while always incorrect in detail (due to scaling problems of strength, gravity, grain size, and related aspects), often provide interesting suggestions and ideas that can then be tested by detailed field observations as well as analytical and/or (depending on the complexity of the problem) numerical models.

For the 2009 episode, Xu et al. (2016) provide an analogue model to explain some aspects of the evolving surface deformation induced by the inferred dyke emplacement. They use crushed silica powder as an analogue for the host rock layers of the dyke. The model is 15 cm wide, 25 cm long, and 12.5 cm thick. The thickness of the layer of crushed silica powder is such that 2.5 cm in the model corresponds to 1 km in the field. They do not explicitly state the depth of the dyke tip below the surface, but from their fig. 5c one can infer that the dyke tip varies (as an 'arc') from a depth of about 3.6 km to, a minimum, of about 1 km below the surface. Xu et al. (2016) then gradually increase the opening, or thickness, of the dyke from 0 cm to a maximum of 0.6 cm and record the associated surface deformation.

Briefly, the main relevant results of the experiments are as follows. At dyke opening of 0.15 cm, there is still no surface faulting. The first faults at the surface appear when the dyke opening has reached 0.3 cm. The surface faults then continue to develop and link up into larger faults as the dyke opening is increased from 0.3 cm to 0.45 cm, and then to 0.6 cm.

These results are interesting, particularly when scaled to the corresponding dimensions in the field. Given that 2.5 cm in the model corresponds to 1 km, a dyke opening or thickness of 0.15 cm should correspond to 60 m. The first fault is seen when the dyke opening or thickness has reached 0.3 cm, which corresponds to a 120 m thick dyke. The final dyke opening of 0.6 cm in the model would correspond to 240 m thick dyke in the field.

That a 60 m thick dyke with a tip at a minimum depth of 1 km depth is unable to generate fractures at the surface is a remarkable result, as is the conclusion that the dyke thickness needs to reach 120 m for the first surface faults to form. These results suggest that only very thick intrusions, or thinner intrusions but very close to the surface, can induce surface fractures. In the paper by Xu et al. (2016) the dyke inferred to be emplaced during the 2009 episode has an opening of about 2 m, while Baer and Hamiel (2010) suggest a general dyke opening of 1-2 m and Pallister et al. (2010) an opening from less than 1 m to a maximum of 4 m. The dyke opening in the analogue model of Xu et al. (2016) at the time of first surface

fault formation is thus 30-100 times greater than that of the dyke, as modelled from deformation data, and 10-20 times greater than the dyke thickness calculated in the present paper.

The analogue models, even if they have little in common with the inferred dyke emplacement during the 2009 episode, illustrate well-known points from both field observations and numerical models. The first point is that there is normally little or no large-scale faulting observed at the tips of arrested dykes (Figs. 9-12; Gudmundsson, 2003). Many photographs of dyke tips reaching to depths of a few metres below the surface, such as from eruptions in Iceland and Hawaii, also fail to show large-scale grabens; well-known examples being the 2011 eruption in Kilauea and the 1980 eruption in the Krafla volcano in North Iceland. Some feeder-dykes and non-feeders, however, are associated with grabens; but the question remains whether the dyke-generated stresses induced the graben or whether the regional extension that is responsible for the dyke injection in the first place also generated the stresses suitable for graben formation. It is well known that most grabens worldwide, in sedimentary basins, in lava piles, and elsewhere are generated by stress fields that have nothing to do with dyke injections. Also, in volcanic areas such as Iceland, where grabens and normal faults are common, dykes are comparatively rare where normal faults are common, and vice versa (Forslund and Gudmundsson, 1991). The 'graben' in Harrat Lunayyir is located at the top of a regional dome, a ridge, which is 30 km wide and rises some 300 m above the surrounding areas (Baer and Hamiel, 2010). Thus, regional doming, presumably related to magma-pressure changes in a deep-seated reservoir beneath the area, may have contributed to the fracture formation during the 2009 episode, in addition to any contribution from the inferred dyke. Doming and general spreading in volcanic areas is a common reason for fracture formation, particularly the formation of tension fractures and normal faults (Gudmundsson, 1987; cf. Gudmundsson, 1999, 2017).

The second point is that most of the numerical models presented here indicate comparatively low surface stresses when there is any reasonable layering of the crust (Figs. 16-24). The only layered models that indicate high enough stresses so as to generate surface fractures are those where the dyke tip is arrested at a very shallow depth, namely at the depth of 300 m (Figs. 18 and 21). In many cases, to initiate surface fractures the dyke tip would have to be even shallower because the overpressure used here, 6 MPa, is comparatively high for a basaltic dyke at a shallow depth in a continental crust. Negative buoyancy (Eq. 2) of basaltic magma in the uppermost kilometres of a continental crust may reduce the overpressure to a few mega-pascals. Also, layering may reduce the dyke-induced surface stresses, even for dyke tips at the shallow depth of 300 m, to very low values (Fig. 24).

As for the 2009 episode, the dyke continued to expand or inflate after it became arrested (Xu et al., 2016). This indicates that the dyke did not become arrested because of declining overpressure (driving pressure) or because of cooling of its front – mechanisms that are often proposed for dyke arrest – but rather though one of the three principal mechanisms discussed above. That is, the arrest of the dyke was most likely due to one, or a combination, of the following mechanisms: Cook-Gordon delamination, stress barrier, and elastic mismatch. All these mechanisms depend on the dyke tip meeting a contact where the arrest occurs – as is, indeed, the most commonly observed condition for dyke arrest in the field (Figs. 9-12; Gudmundsson, 2003, 2011b). Thus, because the mechanical conditions at and above the

contact where the dyke becomes arrested do not allow the dyke to continue on its vertical path, irrespective of its overpressure, the dyke can expand and still stay arrested.

Since the dyke continued to expand after it became arrested, it must have maintained its connection with its source reservoir. The depth to the source reservoir is not well constrained but thought to be somewhere between 20 km and 35 km (Xu et al., 2016). Despite the fact that the dyke must have extended to the depth of at least 20 km, and perhaps 35 km, elastic half-space dislocation modelling detects dyke opening primarily between the depth of 2 km and 7 km, with a maximum opening of 2.3 m, with little modelled opening below 7 km (Xu et al., 2016). Similarly, little opening was detected above 2 km, even if the top of the dyke, in that model, is assumed to have reached the depth of 1 km below the surface.

These results indicate that a dislocation in an elastic half space is a poor model for the dyke. Not only is it clear that the model captures basically only a part of the vertical dyke dimension (the uppermost part and the lower half or two-thirds are mostly missing from the model), but the model cannot explain why the dyke became arrested in the first place. Graben subsidence may contribute to dyke arrest (Gudmundsson, 2003), but in the 2009 episode there was no real graben subsidence because there were no major normal-fault slips at the eastern boundary of the 'graben', only tension fractures. For an overpressured dyke such as here, witness its continued expansion subsequent to arrest, the only known effective mechanisms of arrest are the three listed above, and all require mechanical layering with contacts in-between the layers. In the elastic half-space dislocation model there is absolutely no reason why the dyke should not have reached the surface. The fact that the dyke did not reach the surface clearly indicates a strong layering and local stresses that contributed to its arrest.

Some authors simulate the dyke geometry by dividing the dislocation model into 1 km × 1 km segments or patches, so as to allow for variation in dyke opening. That approach has been used for the dyke emplaced in Harrat Lunayyir in 2009 (Xu et al., 2016). Field measurements of regional dykes of these types, however, show that the thickness variations along strike is generally on the length scale of tens of metres (Delaney and Pollard, 1981; Gudmundsson et al., 2012). The tens-of-metre thickness variation along strike can sometimes been 'smoothed' to one to a few hundred metres (Delaney and Pollard, 1981), but we are not aware of any dykes that fit with the kilometre-scale thickness variation along strike. The measured strike variations in the examples cited above are mostly in mechanically similar host rocks (basaltic lava flows in Iceland and sedimentary rocks in the USA), so that the thickness variation is less than would be in case of greater heterogeneity in the mechanical properties of the host rock in the direction of strike. Variations on the scale of tens of metres in the opening and/or displacement on many kilometre long normal faults are also common and widely observed (Gudmundsson, 2011a). Such variations in displacements on fractures of any size are perhaps best analysed through Fourier series (Kusumoto and Gudmundsson, 2014).

The mechanical host-rock variations are normally much greater in the dip direction than in the strike direction. This follows because the host rock is layered, with great differences in stiffness between the layers (e.g., Figs. 9, 10, and 12). The real mechanical layering – primarily the variation in stiffness or Young's modulus – basically coincides with the natural layering of the rocks as seen in the field in young and highly active volcanic zones and fields

- although in seismic layering, grouping together many similar rock layers is common. For a typical lava pile, the lava thicknesses are commonly 5-20 m and that would correspond to the main thickness variation in the dyke. Occasionally, there are thick pyroclastic or pahoehoe layers or intrusions, some of which may exceed one hundred metres in thickness, and the dykes could be of essentially uniform thickness inside some of those layers or units. Also, as a volcanic zone evolves, some mechanical layers or units may become thicker though mechanical homogenisation of the layers (Gudmundsson, 2011a), and dykes that dissect such layers/units may show litttle thickness variation in the dip direction for several hundred metres. But this applies to few and late-formed dykes in any given volcanic area – and primarily basaltic lava piles. Thus, normally, the thickness variation in the dip direction scales with the thicknesses of the layers that constitute the host rock, most commonly on the order of metres to one to a few tens of metres. Dividing dyke-dislocation models into patches of one square kilometre is thus normally not in harmony with the actual thickness variation of the dyke.

9.3 Interpretation of the 2009 episode

Based on the discussion above, as well as our field observations, analytical models, and numerical models, we interpret the 2009 Harrat Lunayyir episode as follows.

1. There was a regional dyke injection during the episode. The dyke had plenty of overpressure (driving pressure) so as to be potentially able to reach the surface, but became arrested at a shallow depth – most likely at a depth of a few hundred metres below the surface.
2. The arrest, almost certainly, occurred as the dyke tip met a contact between mechanically dissimilar layers. The detailed mechanism of arrest was one, or a combination, of the following: Cook-Gordon delamination, stress barrier, and elastic mismatch.
3. We estimate the dimensions of the dyke from seismic and geodetic data provided in the cited literature on this episode, combined with well-tested fracture-mechanics models and field studies of regional dykes. Our results as regards strike dimension (length) and dip dimension (height) are similar to those of earlier studies. We conclude that the strike dimension is about 14 km and the dip dimension at least 20 km. For the shallow depth of the dyke, the top parts, we estimate the maximum thickness in the range of 5.8-11.6 m or, given the inaccuracy in the estimated Young's moduli and overpressure, somewhere between 6 and 12 m. This is in contrast to the maximum thickness of 2-2.3 m obtained in earlier studies. However, our results fit much better with actual field measurements of the length/thickness ratios of regional dykes worldwide.
4. The tip of the dyke became arrested, not at a depth of 1-2 km, but rather at a depth of a few hundred metres. Our numerical and analytical results indicate that a dyke arrested at 1-2 km depth, as suggested in earlier studies, in a reasonably layered crust and with a typical magmatic overpressure could not induce significant fracture formation at the surface.

5. From the size and shape of the zone of fractures at the surface (Fig. 8) we conclude that a single dyke, whether its tip was arrested at 1 km or at 300 m depth, could not have induced all the fractures. This follows from the distance between the peaks of the surface stresses/surface deformation induced by a dyke – in the absence of an open contact - being roughly double the depth to the tip of the dyke (Figs. 12-24). This means that a dyke with an arrested tip at 1 km depth could explain a 2-km-wide fracture zone at the surface, and a dyke with a tip at 300 m depth could explain a 0.6-km-wide fracture zone. Since the 'graben' or fracture zone generated in the 2009 episode is 3 and 7 km wide, the dyke tip would have to be as deep as 3.5 km to generate it, and the stresses induced by such a deep dyke in a reasonably layered crust are simply far too low to generate the observed fractures.
6. Based on the inferred strike of the dyke, if not its inferred location (Fig. 8), we incline to the view that some of the fractures on the eastern side of the fracture zone or 'graben' were initiated by the dyke-induced stresses. Many of these are tension fractures, and their overall direction fits reasonably well with the inferred strike of the dyke. The projection of the dyke onto the surface, however, is likely to be in an error if this interpretation is correct, meaning that the real dyke was located somewhat further to the east. By contrast the directions of the fractures on the western side of the fracture zone fit poorly with the inferred strike of the dyke. The local direction of extension in the uppermost layers, above the dyke, may have been different from those in some or all the layers through which the dyke propagated. Rotations of the strike of the minimum principal stress σ_3 are common in layered rocks and well known from sedimentary basins and volcanic rift zones (Gudmundsson, 2011a). Such a rotation, if it occurred, would contribute to the condition for dyke arrest and also to the variation in the orientation of normal faults and tension fractures seen in Fig. 8.
7. One possibility that might be considered for the dyke to have induced all the fractures is a weak contact at shallow depths that opens up as the dyke approaches (basically the Cook-Gordon delamination). Then the stresses induced by the dyke concentrate at and above the lateral ends of the contact (Gudmundsson, 2003), so that, theoretically, the distance between the stress peaks could be anywhere between 3 km and 7 km (or wider or narrower depending on the lateral dimension of the open contact). However, for such conditions, the stress peaks at the surface are commonly narrow – a few hundred metres – and low in magnitude (Gudmundsson, 2003), and would thus not ideally fit with the 2-3 km wide zone of fracture formation on the eastern side of the fracture zone in Fig. 8.
8. In this interpretation, a considerable part of the surface fracturing relates to the tectonic stresses in the Harrat Lunayyir area. Relative tension due to some sort of spreading and/or doming (the fracture zone/graben is in the top of a 30 km wide volcanic ridge rising 300 m above its surroundings (Baer and Hamiel, 2010)), is normally a necessary condition for a dyke to form in the first place (Gudmundsson, 2011a). Thus, before the dyke was injected, there existed a local stress field in the area that favoured the formation of normal faults and tension fractures. As the dyke propagated to shallower depths, the local stresses became concentrated in the strip of land above the tip of the dyke. And these stresses are in addition to any stresses

induced by the magmatic overpressure in the dyke. Depending on the layering and contacts above the dyke, these stresses could have generated normal faults and/or tension fractures, in additions to those directly induced by the magmatic overpressure of the dyke itself.

It is perhaps worth emphasising that in volcanotectonic rift zones, dyke intrusion, tension fracturing and normal faulting all connect to the same general loading; namely, horizontal extension across the rift zone. Thus, all these types of fractures occur in rift zones, and often simultaneously during volcanotectonic events, without one type of fracture necessarily triggering another type. It is worth remembering that the formation of most grabens, and normal faults in general, has nothing to do with dyke emplacement. Sedimentary basins are characterised by normal faults and numerous grabens, few if any of which have anything to do with dykes. Thus, as indicated in point 9 above, normal faults, grabens, and dykes partly due to loading through extension, either spreading of some sort or doming or both.

An additional point concerns the difference between half-space models and layered models. In this paper we show that the calculated surface stresses depending strongly on the assumed layering of the crust hosting the dyke. In particular, elastic half-space models, which assume that the crust is non-layered and thus use a uniform average Young's modulus, yield much higher tensile and shear stresses at the surface, for a given dyke overpressure or opening and depth, than models with a crust of alternating stiff and comparatively soft (compliant) layers.

One consequence of using elastic half-space models is that they tend to underestimate the thicknesses of the dykes supposed to induce the surface stresses and deformation. This follows because in half-space models the assumed uniform Young's modulus for the entire crustal segment hosting the dyke is normally much higher than that of the actual shallow layers close to the surface of an active volcanic zone or a volcano. Since there are no soft or compliant pyroclastic, sedimentary, or soil layers in the half-space model, there is no major stress dissipation; the models thus exaggerate the stresses transferred to the surface, and the associated deformation (cf. Figs. 13-15 and Figs. 22-24). Consequently, in a half-space model a thin dyke (normally a dyke with a low overpressure for its given dimensions) at a comparatively large depth can induce large stresses and deformation at the surface. Half-space models thus yield length/thickness or length/height (aspect) ratios of dykes that disagree with direct field studies of dykes as well as with standard fracture-mechanics models.

10. Summary and conclusions

The main conclusions may be summarised as follows.

- Mechanical layering has great effects on dyke-induced stresses and associated surface deformation. Even if the layering details are commonly unknown for volcanic areas, adding plausible general layering, using information from field observations of similar, well-exposed fossil volcanic zones, is likely to yield more realistic results as to surface stresses and deformation than non-layered models such as elastic half-space models.

- Half-space models, such as are commonly used for modelling arrested dykes, can be highly misleading, especially as regards dyke thicknesses. In particular, these models tend to (1) underestimate the dyke thickness so as to yield length (strike)/thickness ratios that are much larger than actually observed in the field and (2) overestimate the likely depth to the tip of a dyke that is supposed to induce a particular surface deformation.
- In the absence of mechanically weak (low tensile strength) or open contacts, the distance between the two dyke-induced surface stress peaks, tensile and shear stresses (and thus, normally, the main surface fractures, if formed) is roughly double the depth to the tip of the arrested dyke. In a reasonably layered volcanic zone/volcano, a typical dyke would rarely induce fractures (if at all) until its tip was as shallow as a few hundred metres or less. This means that any graben or fracture zone induced by the dyke would normally not be wider than several hundred metres.
- In case there is an open contact between layers of the host rock of the dyke, the depth to the dyke tip has no relation to the distance between the stress peaks or graben width at the surface.
- As for the 2009 Harrat Lunayyir episode, we conclude that both dyke emplacement and normal faulting were partly triggered by a regional extensional loading. Furthermore, part of the surface fracturing was the result of dyke-induced stresses. Based on inferred dyke orientation in relation to the fracture pattern, it is likely that primarily the fractures on the eastern side of the fracture zone/graben where thus formed.
- Based on numerical results, we infer that the dyke tip became arrested at a depth of only a few hundred metres. This means that the hazard during the 2009 episode was considerable since the dyke propagation halted only a few hundred metres below the surface. Most likely, the dyke became arrested at a contact between layers of widely different mechanical properties. This follows partly because the dyke thickness continued to increase after it became arrested, and yet the tip was not able to break through the arrester.
- From the inferred depth of the dyke dip it follows that the dyke-induced zone of fractures at the surface is most likely several hundred metres wide. We conclude that the dyke, on its own, could not have generated the entire 3-7 km wide fracture zone associated with the 2009 episode. Much of that fracturing must be directly related to the regional extension and/or doming in the area.
- Using analytical models, we estimate that thickness of the dyke at shallow depths as being in the range of 6-12 m. From seismic data we infer the strike dimension (length) of the dyke as 14 km and the dip dimension or depth as in excess of 20 km. From these results we calculate the length/thickness ratio of the dyke as between about 2400 and 1200, which is similar to the results of field measurement of the length/thickness ratios of dykes exposed at shallow depths in many palaeovolcanic zones.

Acknowledgements

AAS thanks Morayyea Al-Shahrani President of the General Commission of Survey for helpful suggestions and Zohair Nawab, President of Saudi Geological Survey, for help during her fieldwork in Harrat Lunayyir. She also thanks Adel Alsharif, Basim al Dahri, Hani Zahran for help with the field work. Abdullah Al-Amri, Sigurjón Jónsson, Abdullah AlRajehi, Mohammed Moufti, Nabil El-Masry, Maher Al Dahry, Basim Al Dahry, Talal Al Shafi, Yahya al Shehri, Mohammed al farhan, Abdelsalam Elshaafi, and John Browning are thanked for various helpful suggestions and information in connection with this work. The authors thank Alessandro Tibaldi and an anonymous reviewer for helpful review comments.

References

Agustsdottir, T., Woods, J., Greenfield, T., Green, R.G., White, R.S., Winder, T., Brandsdottir, B., Steinthorsson, S., Soosalu, H., 2016. Strike-slip faulting during the 2014 Bardarbunga-Holuhraun dike intrusion, central Iceland. Geophys. Res. Lett., 43, 1495-1503, doi: 10.1002/2015GL067423.

Al Amri, A., Fnais, M., 2009. Seismo-volcanic investigation of 2009 earthquake swarms at Harrat Lunayyir (Ash Shaqah), Western Saudi Arabia. Int. J. Earth Sci. Eng., October issue, 1-18.

Al Amri, A., Fnais, M., Abdel-Rahma, K., Mogren, S., Al-Dabbagh, M., 2012. Geochronological dating and stratigraphic sequences of Harrat Lunayyir, NW Saudi Arabia. International Journal of Physical Sciences. 7, 2791-2805.

Al-Amri, A.M., Al-Mogren, S.M.,2011. Seismo-volcanic investigation of the current activity in Harrat Lunayyir, Al-Madinah Al-Munawwarah area. Final report. King Saud University, Riyadh, 1-184.

Al Damegh, K., Sandvol, E., Barazangi, M., 2005. Crustal structure of the Arabian plate: new constraints form the analysis of teleseismic receiver functions. Earth Planet. Sci. Lett., 231, 177-196.

Al-Zahrani, H., Al-Amri, AM., Abdel-Rahman, K., Fnais, M., 2013. Aftershock sequence analysis of 19 May, 2009 earthquake of Lunayyir lava flow, northwest Saudi Arabia. Inter. J. Physical Sci. 8, 277-285.

Baer, G., Hamiel, Y., 2010. Form and growth of an embryonic continental rift: InSAR observations and modelling of the 2009 western Arabia rifting episode. Geophysics. J. Int. 182, 155-167.

Bailey, G., 2009. The Red Sea, coastal landscapes and hominin dispersals. In: Petraglia MD, Rose JI (eds) The evolution of human populations in Arabia. Springer, Dordrecht . 15–37.

Barnett, Z.A., Gudmundsson, A., 2014. Numerical modelling of dykes deflected into sills to form a magma chamber. J. Volcanol. Geotherm. Res., 281, 1-11.

Becerril, L., Galindo, I., Gudmundsson, A., Morales, J.M., 2013. Depth of origin of magma in eruptions. Scientific Reports 3, 2762. doi: 10.1038/srep02762

Brown, G., Hedge, C., Marvin, R., 1978. Geochronologic data for the Arabian Shield. Section 2.Tabulation of Rb-Sr and K-Ar ages given by rocks of the Arabian Shield. US Geological Survey Saudi Arabian Project Report . 240-20.

Camp, E., Roobol, J., 1992. Upwelling asthenosphere beneath western Arabia and its regional implications. J. Geophys. Res., 97, 15,255-15,271

Casagli N., Tibaldi A., A. Merri, C. Del Ventisette, T. Apuani, L. Guerri, J. Fortuny-Guasch, D. Tarchi, 2009. Deformation of Stromboli Volcano (Italy) during the 2007 eruption revealed by radar interferometry, numerical modelling and structural geological field data. J. Volcanol. Geotherm. Res., 182, 3–4, 182-200.

Cochrna, R., Karner, D., 2007. Constraints on the deformation and rupturing of continental lithosphere of the Red Sea: the transition from rifting to drifting. Geol. Soc. Lond., Spec. Pub. 282, 265-289.

Delaney, P.T., Pollard, D.D., 1981. Deformation of host rock and flow of magma during growth of minette dike and breccia-bearing intrusions near Ship Rock, New Mexico. U.S. Geol. Surv. Prof. Pap. 1202, 1-69.

Duncan, A., Al-Amri, M., 2013. Timing and composition of volcanic activity at Harrat Lunayyir, western Saudi Arabia. J. Volcanol. Geothermal. Res., J. Volcanol. Geothermal Research . 260,103–116.

Dzurisin, D., 2006. Volcano Deformation. Springer Verlag, New York.

Forslund, T., Gudmundsson, A., 1991. Crustal spreading due to dikes and faults in southwest Iceland. J. Struct. Geol., 13, 443-457.

Garcia, A. Ortiz, R., Marrero, J.M., Sanchez, N., Tarraga, M., Vila, J., Correig, Macia, R., Sleeman, R., 2006. Monitoring the reawakening of Canary Islands' Teide Volcano. Eos, 87, 61-72.

Genna, A., Nehilg, P, Le Goff, E., Guerrot, C., Shanti, M., 2002. Proterozoic tectonism of the Arabian Shield. Precam. Res., 117, 21–40.

Gonnermann, H.M., Manga, M., 2013. Dynamics of magma ascent in the volcanic conduit. In: Fagents, S.A., Gregg, T.K.P., Lopes, R.M.C. (eds), Modeling Volcanic Processes. Cambridge University Press, Cambridge, pp. 55-84.

Gottsmann, J., Wooller, L., Marti, J., Fernandez, J., Camacho, A.G., Gonzalez, P.J., Garcia, A., Rymer, H., 2006. New evidence for the reawakening of Teide volcano. Geophys. Res. Lett., 33, L20311, doi:10.1029/2006GL027523.

Greenland, L.P., Rose, W.I., Stokes, J.B., 1985. An estimate of gas emissions and magmatic gas content from Kilauea volcano. Geochim. Cosmochim. Acta, 49, 125-129.

Greenland, L. P., Okamura, A. T., Stokes, J. B., 1988. Constraints on the mechanics of the eruption. In: Wolfe, E. W (ed), The Puu Oo Eurption of Kilauea Volcano, Hawaii: Episodes Through 20, January 3, 1983 Through June 8, 1984, US Geol. Survey Professional Paper, 1463, 155–164.

Gudmundsson, A., 1986. Formation of crustal magma chambers in Iceland, Geology, 14, 164-166.

Gudmundsson, A., 1987. Geometry, formation and development of tectonic fractures on the Reykjanes Peninsula, Southwest Iceland. Tectonophysics, 139, 295-308.

Gudmundsson, A., 1999. Postglacial crustal doming, stresses and fracture formation with application to Norway. Tectonophysics, 307, 407-419.

Gudmundsson, A., 2002. Emplacement and arrest of sheets and dykes in central volcanoes. J. Volcanol. Geotherm. Res., 116, 279-298.

Gudmundsson, A., 2003. Surface stresses associated with arrested dykes in rift zones: Bull. Volcanol., 65, 606-619.

Gudmundsson, A., 2011a. Rock Fractures in Geological Processes. Cambridge University Press, Cambridge.

Gudmundsson, A., 2011b. Deflection of dykes into sills at discontinuities and magma-chamber formation. Tectonophysics, 500, 50-64.

Gudmundsson, A., 2012. Magma chambers: formation, local stresses, excess pressures and compartments. J. Volcanol. Geotherm.Res., 237-238, 19–41.

Gudmundsson, A., 2017. The Glorious Geology of Iceland's Golden Circle. Springer-Nature, Heidelberg.

Gudmundsson, A., Friese, N., Galindo, I., Philipp, S.L., 2008. Dike-induced reserve faulting in a graben. Geology, 36, 123-126, doi: 10.1130/G24185A.

Gudmundsson, A., Loetveit, I.F., 2005. Dyke emplacement in a layered and faulted rift zone. J. Volcanol. Geotherm. Res. 144, 311-328.

Gudmundsson, A., Philipp, L., 2006. How local stress fields prevent volcanic eruptions. J. Volcanol. Geotherm. Res . 158, 257-268.

Hansen, E., Puckett, E., Keller, R., Brueseke, E., Bulen, L., Mertzman, A., Finegan, A., McCleery, A., 2013. Intra-plate magmatism related to opening of the southern Iapetus Ocean: Cambrian Wichita igneous province in the Southern Oklahoma rift zone. Lithos, 174, 57–70.

Hansen, E., DeShon, R., Driskell, M., Al-Amri, M., 2013. Investigating P-wave velocity structure beneath Harrat Lunayyir, northwestern Saudi Arabia, using double-difference tomography and earthquakes from the 2009 seismic swarm. J. Geophys. Res., 118, 4814-4826, 10.1002/jgrb.50286.

Hosny, A., Nyblade, A., 2014. Crustal structure in southeastern Egypt: symmetric thinning of the northern Red Sea rifted margins. Geology, 42, 219-222, doi.org/10.1130/G34726.1.

Johnson, P.R., Woldehaimanot, B., 2003. Development of the Arabian-Nubian Shield: perspectives on accretion and deformation in the northern East African Orogen and the assembly of Gondwana. In: Windley, M., Dasgupta, S. (eds), Proterozoic East Gondwana: Supercontinent Assembly and Breakup. Geol. Soc. Lond. Spec. Pub. 206, 289-325.

Jonsson, S., 2012. Tensile rock mass strength estimated using InSAR. Geophys. Res. Lett., 39, L21305, doi:10.1029/2012GL053309.

Kavanagh, J., Menand, T., Sparks, R.S.J., 2006. An experimental investigation of sill formation and propagation in layered elastic media. Earth Planet. Sci. Lett., 245, 799-813.

Keir, D., Pagli, C., Bastow, I., Ayele, A., 2011. The magma-assisted removal of Arabia in Afar: Evidence from dyke injection in the Ethiopian rift captured using InSAR and seismicity. Tectonics, 30, doi:10.1029/2010TC002785.

Koulakov, I., El Khrepy, S., Al Arifi, N., Sychev, I., Kuznetsov, P., 2014. Evidence of magma activation beneath the Harrat Lunayyir basaltic field (Saudi Arabia) from attenuation tomography. Solid Earth . 5, 873–882.

Kusumoto, S., Gudmundsson, A., 2014. Displacement and stress fields around rock fractures opened by irregular overpressure variations. Front Earth Sci., 2, doi: 10.3389/feart.2014.00007.

Moran, S.C., Newhall, C., Roman, D.C., 2011. Failed magmatic eruptions: late-stage cessation of magma ascent. Bull. Volcanol., 73, 115-122, doi: 10.1007/s00445-010-0444-x.

Mukhopadhyay, B., Mogren, S., Mykhopdadhyay, M., Dasgupta, S., 2013. Incipient status of dyke intrusion in top crust – evidences from the Al-Ays 2009 earthquake swarm, Harrat Lunayyir, SW Saudi Arabia. Geomat, Nat. Haz. and Risk, 4, 30-48.

Pallister, J., McCausland, W., Jónsson, S., Lu, Z., Zahran, H., El-Hadidy, S., Aburukbah, A., Stewart, I., Lundgern, P., White, R., Moufti, M., 2010. Broad accommodation of rift-related extension recorded by dyke intrusion in Saudi Arabia. Nat. Geosci . 8.

Pint, J., 2006. Vulcanospeleology in Saudi Arabia. UIS Commission on Volcanic Caves.

Powers, W., Ramirez, F., Redmond, D., Elberg, L., 1963. Geology of the Arabian Peninsula Sedimentary Geology of Saudi Arabia. U.S. GEOLOGICAL SURVEY

Rehman, S., 2010. Saudi Arabian Geothermal Energy Resources-an Update. World Geothermal Congress, Bali, Indonesia.

Rickwood, P.C., 1990. The anatomy of a dyke and the determination of propagation and flow directions. In: Parker, A.J., Rickwood, P.C., Tucker, D.H. (eds), Mafic Dykes and Emplacement Mechanisms. Balkema, Rotterdam, 81-100.

Rivalta, E., Taisne, B., Bunger, P., Katz, F., 2015. A review of mechanical models of dyke propagation: Schools of thought,results and future directions. Science Direct ,Tectono physics. 638, 1-42, doi.org/10.1016/j.tecto.2014.10.003.

Rodgers, J., Walter, R., Mellors, J., Al-Amri, M., 1999. Lithospheric structure of the Arabian Shield and Platform from complete regional waveform modelling and surface wave group velocities, Geophysics. J. Int . 138, 871–878.

Segall, P., 2010. Earthquake and Volcano Deformation. Princeton University Press, Princeton.

Sigmundsson, F., Hreinsdottir, S., Hooper, A., Arnadottir, T., Pedersen, R., Roberts, M.J., Oskarsson, N., Auriac, A., Decriem, J., Einarsson, P., Geirsson, H., Hench, M., Ofeigsson, B.G., Sturkell, E., Sveinbjörnsson, H., and Feigl, K.L., 2010. Intrusion triggering of the 2010 Eyjafjallajökull explosive eruption. Nature, 468, 426-430, doi:10.1038/nature09558.

Stern, J., 2008. Neoproterozoic crustal growth: the solid Earth system during a critical episode of Earth history. Gondwana Research. 14, 33–50.

Stern, R., Johnson, P., 2010. Continental lithosphere of the Arabian Plate; a geologic, petrologic, and geophysical synthesis. Earth-Sci Rev. 101, 29-67.

Tibaldi A., 2015. Structure of volcano plumbing systems: A review of multi-parametric effects. J. Volcanol. Geotherm. Res., 298, 85–135.

Tibaldi A., Pasquarè F., 2008. A new mode of inner volcano growth: The “flower intrusive structure”. Earth Planet. Sci. Lett., 271, 202-208.

Townsend, M.R., Pollard, D.D., Smith, R.P., 2017. Mechanical models for dikes: A third school of thought. Tectonophysics, 703-704, 98-118,

Waltham, T., 2005. Extension tectonics in the Afar Triangle. Geology Today, 2005, 10.1111/j.1365-2451.2005.00510.x

Zobin, V., Al-Amri, A., Fnais, M., 2013. Seismicity associated with active, new-born and re-awakening basaltic volcanoes: case review and the possible scenarios for the Harrat volcanic provinces, Saudi Arabia. Arab J Geosci. 6, 529–541.

Xu, W., Jonsson, S., Corbi, F., Rivalta, E., 2016. Graben formation and dike arrest during the 2009 Harrat Lunayyir dike intrusion in Saudi Arabia: insights from InSAR, stress calculations and analog experiments. J. Geophys. Res., 121, doi:10.1002/2015JB012505

.